Rigorous Numerical Methodology and Heat Recovery Analysis for Modeling of Direct Use Geothermal Systems

Chen, Yuan; Voskov, Denis; Daniilidis, Alexandros

DOI
10.1016/j.geoen.2025.213661

Publication date
2025

Document Version
Final published version

Published in
Geoenergy Science and Engineering

247 (2025) 213661

Contents lists available at ScienceDirect

Geoenergy Science and Engineering

journal homepage: www.sciencedirect.com/journal/geoenergy-science-and-engineering

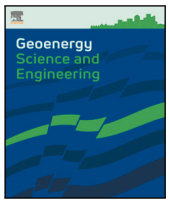

Rigorous Numerical Methodology and Heat Recovery Analysis for Modeling of Direct Use Geothermal Systems

Yuan Chen [a,*], Denis Voskov [a,b], Alexandros Daniilidis [a]

[a] Department of Geoscience & Engineering, TU Delft, Stevinweg 1, 2628 CN Delft, Netherlands
[b] Department of Energy Science & Engineering, Stanford University, Stanford, CA 94305, USA

ARTICLE INFO

Dataset link: https://gitlab.com/open-darts/darts-models/

Keywords:
Direct-Use Geothermal Systems
Geological heterogeneity
Open-source software
Optimal numerical setup
Heat in place recovery factor
Distance-based Generalized Sensitivity Analysis

ABSTRACT

Direct Use Geothermal Systems (DUGS) are rapidly and densely deployed to meet the growing demand for renewable energy with less carbon emissions globally. The simulation of DUGS can provide a reservoir-scale understanding of geothermal resource assessment, where the geothermal system's lifetime and the injection well Bottom Hole Pressure (BHP) are used as performance indicators. However, there are inherent errors from numerical simulations of any engineering problems, due to approximating continuous partial differential equations by their discretized approximation in time and space. In this work, we establish an optimal numerical setup with reduced errors across the homogeneous, stratified and heterogeneous models for the simulation of a geothermal system. Next, we develop a standardized method for calculating recoverable Heat In Place (HIP) and an analytical solution for evaluating the HIP recovery factor across various geological models using a single forward simulation. We present reference examples on the design of DUGS simulations using the open-source software Delft Advanced Research Terra Simulator (open-DARTS). The open-DARTS platform enables accurate and efficient sensitivity and uncertainty analysis. Using Distance-Based Generalized Sensitivity Analysis (DGSA), we identify reservoir depth and discharge rate as the most influential parameters for geothermal projects across all three types of geological models.

1. Introduction

Greenhouse gas (GHG) emissions and high energy demand are key societal concerns nowadays. Renewable energy sources like wind and geothermal energy are increasingly installed to reduce emissions. Geothermal energy includes a wide range of applications, such as electricity generation, ground-source heat pumps, and Direct Use Geothermal Systems (DUGS). DUGS also known as low-enthalpy systems, using injection and production wells to extract geothermal energy. These systems are increasingly installed across Europe, targeting the provision of 20% of the region's total heat demand by 2030 (Bruhn et al., 2022). They are mainly targeting at the deep sedimentary environment, which are water-dominated, at depths around 2 km to 3 km with a temperature below 150 °C (Barbier, 2002). The typical reservoir rock types of these systems are terrestrial fluvial clastic sequence (Moeck, 2014) because of the known good porosity and good permeability.

These systems are influenced by complex subsurface geomechanical, chemical, and multi-physics processes, as well as the intrinsic complexities of geological sedimentary processes, which impact the pore volume, hydraulic connectivity and the fluid properties of the geological reservoir. No simple analytical solution exists for these intricate dynamics.

The design and development of a geothermal project are at an early stage when the availability of subsurface information is limited. Uncertainties at this stage are quite high. The uncertainties come from limited knowledge of the resource estimation, poor understanding of the subsurface, drilling risks, financial and environmental risks which can possibly result in project failure. Numerical simulation is employed to provide crucial inputs for DUGS studies of feasibility and risk at essential phases of projects. It provides a long-term and reservoir-scale understanding of the fluid flow in porous media and the interaction of the injected fluid with rock and in-situ fluid (Pandey et al., 2018). Nevertheless, numerical simulation uses discrete approximation approach to describe a continuous problem. There will be inherent errors in the numerical solution coming from the discretized representation of the continuous system. Truncation error and round-off error are two error types existing in any numerical simulation process. The truncation error can be mitigated by introducing a small step size in space (model

* Corresponding author.
E-mail address: y.chen-21@tudelft.nl (Y. Chen).

https://doi.org/10.1016/j.geoen.2025.213661
Received 21 October 2024; Received in revised form 14 December 2024; Accepted 2 January 2025
Available online 8 January 2025

resolution), while the round-off error can be minimized by using a higher precision arithmetic or more advanced algorithms. A fine resolution makes the simulation time-consuming while the simulation results remain accurate, so it is necessary to find an optimal resolution for a simulation. Significant simulation studies on geothermal applications have been carried out to investigate and quantify the challenges of geothermal systems. Homogeneous (Poulsen et al., 2015; Saeid et al., 2015; Daniilidis et al., 2016; Feng et al., 2017; Daniilidis et al., 2021), stratified (Robert et al., 2022; Tang et al., 2024), and heterogeneous (Seibert et al., 2014; Wang et al., 2021; Blank et al., 2021; Wang et al., 2023; Major et al., 2023) geological models are created to investigate the dynamic thermal response of geothermal production.

The ideal model has a high accuracy, a low truncation error and is computationally efficient. Homogeneous, stratified and heterogeneous geological models are constructed by multiple grid cells, where each grid cell represents a control volume of the subsurface formation. In numerical simulation, a solution is reached with the construction of discrete grid cells to represent the governing equations in a finite form and to implement relevant boundary conditions (Soni, 2000). There are various grid generation techniques that can be summarized as structured, unstructured, hybrid and gridless. Meanwhile, a Cartesian grid is the simplest structured grid type to discretize the given field imposed by pertinent boundary conditions (Soni, 2000). Besides the simplicity of the Cartesian grid, the intrinsic regularity of the Cartesian grid adds flexibility to deal with high-order numerical problems and to implement parallel processing in later dynamic simulation stages. Model resolution refers to the size of Cartesian grid cells used to represent subsurface geological properties (Ahmed, 2010). Smaller grid cells capture reservoir heterogeneity more accurately but require more computational resources and data, while larger cells offer greater efficiency with less precision. Reservoir engineers balance this trade-off based on available data and computational cost. Despite the inherent complexities of sedimentary systems, the representative scale of a model can be determined by the characteristics of geological heterogeneity (Ahmed, 2010).

Confining layers are usually geological formations made up of low-permeability or impermeable rocks that restrict the movement of fluids and reduce heat flow by limiting fluid convection (De Bruijn et al., 2021). Although the low-permeable confining layers prevent fluid flow and convective heat transfer, they provide heat recharge to reservoir layers by heat conduction. Some studies (Crooijmans et al., 2016; Kong et al., 2017) ignore the heat recharge from the confining layers for DUGS simulation investigations. Daniilidis et al. (2020b) shows the less permeable reservoir bodies between more permeable reservoir bodies also have heat recharge effect. Other studies (De Bruijn et al., 2021; Wang et al., 2021) focus on the effect of confining layers proving the positive effect of these layers on heat production. However, not all studies emphasize the addition of the number of confining layers to avoid boundary interaction effects and maintain the accuracy of the simulation while the simulation remains computationally efficient.

There are various open-source and commercial computational tools which are capable of geothermal production simulations (O'Sullivan et al., 2001; Pandey et al., 2018), such as TOUGH2 and its derivatives (Battistelli et al., 1997; Pruess et al., 1999), COMSOL Multiphysics (COMSOL, 2023), ADGPRS (Automatic Differentiation General Purpose Research Simulator) with geothermal module (Voskov and Zhou, 2015; Wong et al., 2015), Matlab Reservoir Simulation Toolbox (MRST) (Lie, 2019; MATLAB, 2020) and Schlumberger Eclipse (Schlumberger, 2023). In this study, the open-source simulator Delft Advanced Research Terra Simulator (open-DARTS) (Voskov et al., 2024b) is used to provide reference examples of the DUGS simulation. Open-DARTS has been applied for various geothermal simulation applications (Khait and Voskov, 2019; Wang et al., 2023; Major et al., 2023) because of its proven efficiency and accuracy in solving complicated multi-phase, multi-component, thermal and chemical fluid flow problems for the given complex geological models. Open-DARTS is a robust and efficient reservoir simulator that can be used to model various energy transition problems. It is implemented using the state-of-arts Operator-Based Linearization (OBL) (Voskov, 2017) framework. The OBL approach discretizes the nonlinear terms within the governing equations and writes the terms in the operator form depending on the physical states. Subsequently, the operators are translated into multi-dimensional tables in the parameter space and then multi-linear interpolation is employed to create a continuous solution during the simulation.

A previous study (Khait and Voskov, 2018) found that the production temperature from open-DARTS simulation with a physical interpolation table of 8 physical points matches the reference result and the performance of simulation remains efficient for a heterogeneous reservoir. It will be meaningful to investigate the optimal OBL physical resolution for different types of reservoir models to maintain the accuracy of the simulation meanwhile the simulation is computationally efficient. The physical parametrization formation simplifies the construction of the Jacobian matrix with the potential extension to advanced parallel computation (Khait and Voskov, 2017; Wang et al., 2023).

Once a geological model with a sufficient resolution and a minimum number of confining layers is determined, it is desired to investigate the potential energy produced from the given geological models subject to uncertain subsurface properties, development parameters and economic inputs (Daniilidis, 2024). The effect of different parameters on thermal response across different types of reservoir models varies. It is imperative to generate reference geothermal simulation examples to include all uncertain parameters and provide geoscientists, engineers and operators with reliable system lifetime and energy production estimations on a DUGS production project.

Previous experimental and numerical studies demonstrated the importance of water density and viscosity changes as a function of temperature to reflect the system lifetime of a deep low-enthalpy geothermal production for the given conceptual homogeneous model (Ma and Zheng, 2010; Watanabe et al., 2010; Saeid et al., 2014). Another study (Saeid et al., 2015) took water salinity into consideration concluding that water salinity adversely affects the energy production and system lifetime of a geothermal operation using a homogeneous 3D model. Meanwhile, Wang et al. (2023) found that the salinity also positively impacts the economic outputs and the energy production of a geothermal simulation for a highly heterogeneous geological model. The study (Daniilidis and Herber, 2017) highlighted the importance of thermal conduction of various rocks for a geothermal system and later (Wang et al., 2023) performed a sensitivity study of heat production with different rock conductivity.

In addition to fluid properties, the characterization of fault throw and fault flow properties have an impact on the geothermal system lifetime. This was investigated using a synthetic layered geological model (Daniilidis et al., 2020b,a). Wang et al. (2023) concluded that the homogeneity of the geological properties leads to a more regular cold plume extent and overestimation on the thermal breakthrough time. Previous work (Saeid et al., 2015) studied solely porosity changes and showed that they result in decreased system lifetime and produced thermal energy.

Saeid et al. (2015) and Daniilidis et al. (2016) investigated the effect of discharge rate, injection fluid temperature, well spacing and the tubing material on thermal breakthrough and the extracted thermal energy for a conceptual homogeneous reservoir.

During geothermal production, hydraulic connectivity near the wellbore is changing. A constant dimensionless variable called well skin factor is used to represent the lumped effects of different parameters on fluid flow performance (Guo et al., 2017).

Subsurface heterogeneity is one of the significant factors affecting DUGS development. It impacts the fluid flow in the geothermal production subsequently affects the thermal response at the production

well (Willems et al., 2017). Flow diagnostics are developed to investigate the reservoir heterogeneity in flow path, well connectivity and drainage/sweeping volume in a streamline simulation (Datta-Gupta and King, 2007; Thiele, 2005). They are based on the quantities of Time Of Flight (TOF) and influence regions deriving from the basic flow simulation (Lie, 2019). The quantities are in cell-wise which represent the average volume over all streamlines to quantify how much fluid can potentially pass through for the given travel time of massless particles (Lie, 2019; Møyner et al., 2015). The average volume can be considered as the region which can be reached by the cold water in a geothermal simulation study.

The wide range of uncertain sources and their interactions make the evaluation of their impact on DUGS thermal model response highly complex. However, there is no clear understanding of the ranking of these parameters subject to the interactions on the thermal response across all types of geological models. Recently, a decision tree-based sensitivity analysis approach has been developed in the subsurface systems' modeling field to deal with continuous and discrete variables (Scheidt et al., 2018). Distance-based Generalized Sensitivity Analysis (DGSA) approach is an extension of regionalized sensitivity analysis (RSA) with the advancement of accepting different distributions of inputs focusing the problems relevant to Earth Sciences (Park et al., 2016). This approach accounts for high-dimensional parameter space and the interactions among parameters, while the process remains computationally efficient. DGSA classifies the responses based on the distance between the input cumulative distribution functions (CDF) and clustering-based CDF to more accurately quantify the importance of different input parameters on the responses. DGSA has been used successfully to study the extraction of geothermal energy from mines (Zhang et al., 2025).

Although open-DARTS has been thoroughly validated against other numerical simulators for geothermal simulation (Wang et al., 2020) and successfully applied to real-world projects: Delft campus geothermal project (Voskov et al., 2024a) and CRECCIT project (Wang et al., 2021), there remains a lack of a general methodology for modeling DUGS. In this paper, we present the general framework of computationally efficient DUGS simulations, designed to minimize numerical errors across all geological models with the open-DARTS. Additionally, we propose a standardized geothermal resource assessment method to defining the effective Influence Area (IA) subsequently to calculating recoverable Heat In Place (HIP) and HIP recovery factor. At the end, we conduct a comprehensive sensitivity analysis for DUGS with an optimal numerical setup, enabling us to rank the importance of different parameters in DUGS development.

2. Methods

We first introduce the numerical model followed by the geological model, then we explain how to perform the standardized flow diagnostic from MRST (Møyner et al., 2015) to define the effective Influence Area (IA) to compute recoverable HIP and then we show the impact of different parameters on thermal response using DGSA.

2.1. Numerical model

In this study, we employ generic multiphase multi-component energy and mass conservation equations to represent single-phase pure brine in Direct Use Geothermal Systems (DUGS), using the open-source IAPWS-IF97 package to calculate the thermodynamic properties of water. The detailed spatial discretization, temporal discretization, and linearization approaches will follow.

2.1.1. Mass conservation equation

A general mass conservation equation for a multi-component (n_c) and multi-phase (n_p) geothermal system can be expressed as follows,

$$\frac{\partial}{\partial t}(\phi \sum_{p=1}^{n_p} x_{cp}\rho_p s_p) + div \sum_{p=1}^{n_p} x_{cp}\rho_p s_p \vec{u_p} + \sum_{p=1}^{n_p} x_{cp}\rho_p \tilde{q_p} = 0, c = 1, \dots, n_c \quad (1)$$

here, t [day] is simulation time, x_{cp} [–] is component c concentration in phase p, s_p [–] is saturation of phase p, $\vec{u_p}$ [m s^{-1}] is velocity of phase p, ρ_p represents phase p phase density [kg m^{-3}], $\tilde{q_p}$ [m^3 d^{-1}] is the source term of the phase p, ϕ [–] is effective porosity. Assuming the rock is compressible, the following equation can be applied to evaluate the effective porosity:

$$\phi = \phi_0(1 + c_r(p - p_{\text{ref}})) \quad (2)$$

where ϕ_0 [-] is the initial porosity of the reservoir, c_r [1/bars] is the rock compressibility and p_{ref} [bars] is the reference pressure. Phase velocity follows Darcy's law:

$$\vec{u_p} = -(\mathbf{K}\frac{k_{rp}}{\mu_p}(\nabla p_p - \gamma_p \nabla D)) \quad (3)$$

where $\mathbf{K}$ [mD] is the effective permeability tensor, k_{rp} [–] is phase p relative permeability, μ_p [mPa s] is phase viscosity, p_p [bars] is pressure of phase p, $\gamma_p = \rho_p g$ [N m^{-3}] is vertical pressure gradient and D [m] is depth. After neglecting the capillarity, the finite volume method is employed to discretize the spatial domain on a general structured and unstructured grid, and the backward Euler approach is used to discretize the time domain. The discretized mass conservation equation is

$$V[(\phi \sum_{p=1}^{n_p} x_{cp}\rho_p s_p)^{n+1} - (\phi \sum_{p=1}^{n_p} x_{cp}\rho_p s_p)^n] - \Delta t \sum_l (\sum_{p=1}^{n_p} x_{cp}^l \rho_p^l \Gamma_p^l \Delta\psi^l) + \Delta t \sum_{p=1}^{n_p} x_{cp}\rho_p q_p = 0, c = 1, \dots, n_c \quad (4)$$

here V [m^3] is the control volume, Γ_p^l is the convective transmissibility at the cell interface 1 [mPa s m^2 d^{-1} bar^{-1}], which is the combination of grid geometry and absolute permeability, ψ^l [bars] is the phase pressure, $q_p = \tilde{q_p}V$ [m^3 s^{-1}] is the fluid source/sink.

2.1.2. Energy conservation equation

For a non-isothermal case, the energy conservation equation is introduced:

$$\frac{\partial}{\partial t}(\phi \sum_{p=1}^{n_p} \rho_p s_p U_p + (1-\phi)U_r) + div \sum_{p=1}^{n_p} h_p \rho_p \vec{u_p} + div(\kappa \nabla T) + \sum_{p=1}^{n_p} h_p \rho_p \tilde{q_p} = 0 \quad (5)$$

here, h_p is phase enthalpy [kJ/kg], κ is effective thermal conduction [kJ m^{-1} d^{-1} K^{-1}], U_p [kJ m^{-3}] and U_r [kJ m^{-3}] are phase p specific internal energy of fluid and rock respectively, which are calculated as follows,

$$U_p = \rho_p h_p - p \quad (6)$$

$$U_r = C_r(T - T_{\text{ref}}) \quad (7)$$

where C_r [kJ m^{-3} K^{-1}] is the volumetric heat capacity of rocks. T_{ref} is the reference temperature [K], which is normally 273.15 K for pure water. The same discretization strategy used in discretizing the mass equation is used to discretize the energy conservation equation:

$$V[(\phi \sum_{p=1}^{n_p} \rho_p s_p U_p + (1-\phi)U_r)^{n+1} - (\phi \sum_{p=1}^{n_p} \rho_p s_p U_p + (1-\phi)U_r)^n] - \Delta t \sum_l (\sum_{p=1}^{n_p^l} h_p^l \rho_p^l \Gamma_p^l \Delta\psi^l + \Gamma_c^l \Delta T^l) + \Delta t \sum_{p=1}^{n_p} h_p \rho_p \tilde{q_p} = 0 \quad (8)$$

Γ_c^l is the conductive transmissibility at the cell interface l which is defined as follows,

$$\Gamma_c^l = \Gamma_g^l[\phi\kappa_p + (1-\phi)\kappa_r] \quad (9)$$

where Γ_g^l is the geometry shape coefficient [mPa s m^2] at the cell interface l, κ_p is phase p conductivity [kJ m^{-1} d^{-1} K^{-1}] and κ_r is rock conductivity [kJ m^{-1} d^{-1} K^{-1}].

The above mass conservation and energy conservation equations are solved on the basis of an Operator-based Linearization (OBL) approach in the open-DARTS platform (Voskov et al., 2024b). To apply OBL, the discretized mass conservation Eq. (4) is written in the following operator-based residual form:

$$r(\xi,\omega,\mathbf{u}) = V(\xi)\phi_0(\xi)\left(\alpha(\omega)-\alpha\left(\omega_n\right)\right) - \sum_l \beta^l(\omega)\Delta t\Gamma^l(p^b-p^a)^l + \theta(\xi,\omega,\mathbf{u}) = 0 \tag{10}$$

The operators in Eq. (10) are defined as follows:

$$\alpha(\omega) = \left(1+c_r\left(p-p_{ref}\right)\right)\sum_{p=1}^{n_p} x_{cp}\rho_p s_p, \tag{11}$$

$$\beta(\omega) = \sum_{p}^{n_p} x_{cp}\frac{k_{rp}}{\mu_p}\rho_p, \tag{12}$$

$$\theta(\xi,\omega,\mathbf{u}) = \Delta t\sum_{p=1}^{np} x_{cp}\rho_p q_p(\xi,\omega,\mathbf{u}). \tag{13}$$

From Eqs. (11) to (13), the vector $\mathbf{u}$ contains well-control variables, ω is the set of state variables and ξ are the set of spatial coordinates. In addition, α is the accumulation operator, β is the flux operator, and θ is the source/sink operator.

Similarly, the operator-based residual form of the energy conservation equation is written as follows,

$$r_e(\xi,\omega,\mathbf{u}) = V(\xi)\left(\alpha_e(\omega)-\alpha_e\left(\omega_n\right)\right) - \sum_l \beta_e^l(\omega)\Delta t\Gamma^l(p^b-p^a)^l - \sum_l \gamma_e^l(\omega)\Delta t\Gamma^l(T^b-T^a)^l + \theta_e(\xi,\omega,\mathbf{u}) = 0 \tag{14}$$

where the operators in the Eq. (14) are defined below,

$$\alpha_e(\omega) = \phi\left(\sum_{p=1}^{n_p}\rho_p s_p U_p - U_r\right), \tag{15}$$

$$\beta_e(\omega) = \sum_{p}^{n_p} h_p^l\rho_p^l\frac{k_{rp}^l}{\mu_p}, \tag{16}$$

$$\gamma_e(\omega) = \phi\left(\sum_{p=1}^{n_p} s_p\lambda_p - \kappa_r\right) + \kappa_r. \tag{17}$$

here T_a, and T_b are temperatures in blocks a and b.

The OBL approach is based on a simplified representation of the nonlinear operators in the parameter space of the simulation problem. The fully implicit method (FIM) is utilized for time approximation and the Newton–Raphson method is applied to solve the governing equation Eqs. (10), (14) based on the set of unknowns.

2.2. Geological model

Three different types of conceptual, 3D geological models are considered: (i) homogeneous, (ii) stratified and (iii) heterogeneous are used to look into the simulation reference examples for geothermal applications. All reservoir models have the same domain extending to horizontal by 4500 m × 4200 m, vertical by 100 m. Each model uses a single doublet with mass rate control for both wells and fixed pressure and temperature boundary conditions.

A constant moderate permeability of 800 mD and porosity of 0.2 are assigned to the homogeneous model. Meanwhile, the porosity field of the stratified model is generated for each layer by sampling from a normal distribution with a mean of 0.2 and a standard deviation of 0.06. For the heterogeneous model, Fluvsim (Deutsch and Tran, 2002) is utilized to generate facies distribution to mimic a fluvial depositional system and populate the porosity for a given reservoir geometry. Fluvsim is a specialized open-source object-based modeling program to simulate the fluvial sedimentary systems for the given reservoir geometry, channel sands proportion, levee sands proportion and crevasse splay proportion.

Next, we use a porosity cut-off value of 0.1 to distinguish between shale and sandstone, assigning their respective thermal properties based on this classification. After we get the porosity field of the stratified and heterogeneous model, we applied the Delft sandstone porosity-permeability correlation in Willems et al. (2020) to generate the permeability field. Fig. 1 shows the permeability distribution of the geological models. For all reservoirs, we investigate the optimal Cartesian resolution (OCR) and minimum number of confining layers (MCL) for geothermal simulation without boundary interaction.

The Table 1 shows the hydraulic and design parameters of the models. For constant initial condition, the initial reservoir pressure and temperature are calculated using the hydraulic pressure and thermal gradients at the reservoir bottom depth of 1850 m. While the initial reservoir pressure and temperature of the non-uniform initial condition are populated using the gradients. The gradient-based distribution is the default option for setting the initial condition in this study.

2.3. Effective Influence Area (IA)

The effective Influence Area (IA) is the region between the injection and production wells where the injected cold water can flow and thermal energy can be extracted within the specified geothermal production time. In this study, we define the effective IA of a low-enthalpy geothermal system as the combination of hydraulically connected volume and thermal affected volume of the given geological model. The hydraulic connected volume is determined using the flow diagnostics approach, obtained by assessing the flow behavior of a given reservoir model. The incompressible single-phase without gravity equation Eq. (18) is applied to compute the flow field.

$$\nabla\times\vec{v} = q \tag{18}$$

$$\vec{v} = -\frac{\mathbf{K}}{\mu}\nabla p \tag{19}$$

where $\mathbf{K}$ [mD] is the effective permeability tensor, μ [mPa s] is fluid viscosity, p [bars] is fluid pressure, and q is the injection rate [d^{-1}].

Once the Darcy velocity $\vec{v}$ is determined, the Time-Of-Flight (TOF) is computed for the imaginary particles starting from the injector to a certain position within the reservoir ($\tau_{forward}$) and the imaginary particles reach at the producer from a certain position within the reservoir ($\tau_{backward}$). Following Eqs. (20) and (21) are used to calculate both $\tau_{forward}$ and $\tau_{backward}$.

$$\vec{v}\cdot\tau_{forward} = \phi \tag{20}$$

$$-\vec{v}\cdot\tau_{backward} = \phi \tag{21}$$

where ϕ [-] is the porosity. TOF can provide crucial information on fluid sweeping volume for a fluid flow simulation. Subsequently, the flood volume and drainage volume can be determined using the tracer partitions approach described in Møyner et al. (2015). In this study, the union of flood volume and drainage volume is defined as the hydraulic connected volume for a geothermal simulation, which is denoted as $V_{hydraulic}$ [m^3].

Then, the thermal affected volume denoting as $V_{thermal}$ [m^3] is identified as the volume of blocks that have a one-degree temperature drop compared with the initial reservoir temperature (Babaei and Nick, 2019; Daniilidis et al., 2021; Major et al., 2023). Eq. (22) is applied to get the effective IA of a low-enthalpy geothermal simulation.

$$V_{effective} = V_{hydraulic}\cup V_{thermal} \tag{22}$$

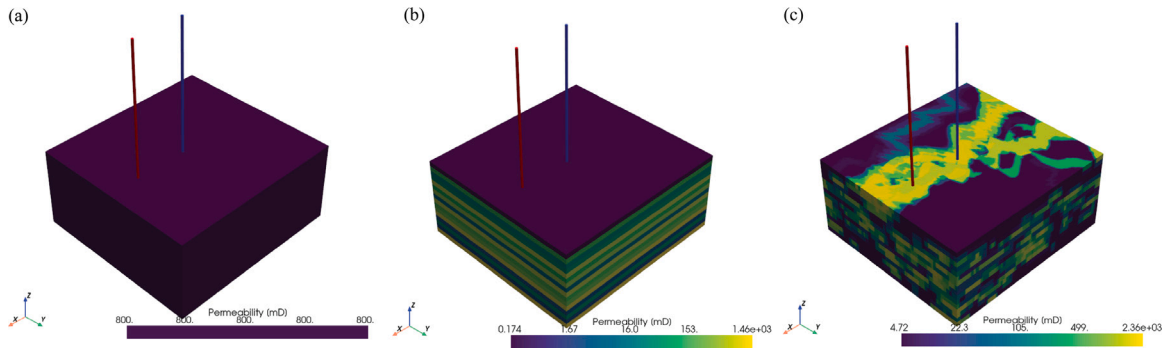

Fig. 1. Permeability distribution of three different conceptual geological models, shown here without confining layers: (a) homogeneous 3D reservoir model, (b) stratified 3D reservoir model and (c) heterogeneous 3D reservoir model. The blue tube in Fig. 1 is the location of the injection well while the red tube indicates the location of the production well.

Table 1
Model parameters.

Parameters	Unit	Values of different types of reservoirs		
		Homogeneous	Layered	Heterogeneous
Porosity	–	0.2	0.06–0.22	0.1-0.27
Permeability	mD	800	0.17–1460	4.27-2350
Reservoir thickness	m		100	
Shale heat capacity	$kJ\,m^{-3}\,K^{-1}$		2300	
Sandstone heat capacity	$kJ\,m^{-3}\,K^{-1}$		2450	
Shale conductivity	$W\,m^{-1}\,K^{-1}$		2.2	
Sandstone conductivity	$W\,m^{-1}\,K^{-1}$		3	
Temperature gradient	$K\,km^{-1}$		30	
Pressure gradient	$bar\,km^{-1}$		107	
Constant initial temperature	K		350	
Constant initial pressure	bar		200	
Discharging rate	$kg\,s^{-1}$		43/86	
Simulation time	years		30	
Well spacing	m		1300	

2.4. Computation of recoverable HIP

The United States Geological Survey (USGS) developed a volumetric methodology to predict the Heat In Place (HIP) which is subject to different sources of uncertainties (Garg and Combs, 2015). The recoverable HIP is defined as heat stored in the reservoir which can be harnessed for power generation or direct use. An operating DUGS is considered to be a forced-convection thermal system, which means the fluid conveys most of the heat produced from the production well. We consider the injection temperature as the reference temperature to compute the recoverable HIP for the given DUGS using following equation (Daniilidis et al., 2021),

$$\text{Recoverable HIP} = \int_0^{V_{\text{effective}}} \left(\left(\rho_w c_w \phi + \rho_r c_r (1-\phi) \right) \left(T - T_{\text{inj}} \right) \right) dV \tag{23}$$

where $V_{effective}$ [m^3] is calculated by Eq. (22), ρ_w and ρ_r are water and rock density [$kg\,m^{-3}$], c_w and c_r are water and rock specific heat capacity [kJ/(kg K)], ϕ [–] is porosity and T_{inj} [K] is injection well temperature.

2.5. Sensitivity analysis

The development of a geothermal project subjects to many uncertain factors from different aspects. These factors are from geological characterization, fluid and rock properties, development plan and operational design. Few studies investigate the joint effect of these factors on geothermal production across all types of geological models.

2.5.1. Distance-based Generalized Sensitivity Analysis (DGSA)

DGSA is based on clustering the responses from the models from multi-dimensional inputs in several groups. The grouping is accomplished by using the kernel techniques such as kernel principal component analysis (KPCA) or kernel clustering (Scheidt and Caers, 2009). Different clusters c_k are created. The L1-norm distance is then computed between the input CDF of each parameter X_i ($F(X_i)$) and the CDF of each parameter in each cluster $c_k (k = 1, 2, 3...C)$ ($F(X_i|c_k)$):

$$\hat{d}_i^k = d_{L_1}(F(X_i), F(X_i|c_k)), \quad k = 1, 2, 3...C; i = 1, \ldots, n \tag{24}$$

Then a bootstrap resampling technique is conducted to check if a parameter X_i has an effect on the response for a response cluster c_k. The resampling creates a distance distribution based on the given percentile α ($\hat{\hat{d}}_{i\alpha}^k$). If the distance of parameter X_i in one cluster c_k ($\hat{d}_i^k$) is larger than the resampling distance distribution $\hat{\hat{d}}_{i\alpha}^k$, it indicates parameter X_i is sensitive, which can be calculated by:

$$\hat{d}_i^{s(k)} = \frac{\hat{d}_i^k}{\hat{\hat{d}}_{i\alpha}^k} \tag{25}$$

The average sensitivity of one parameter X_i on the responses is computed as:

$$s(X_i) = \frac{1}{C} \sum_1^C \hat{d}_i^{s(k)} \tag{26}$$

In this work, we employ the python version of DGSA (pyDGSA) (Perzan, 2024).

3. Results and discussions

We first present the findings on the optimal numerical setup for the three geological models developed for a low-enthalpy geothermal

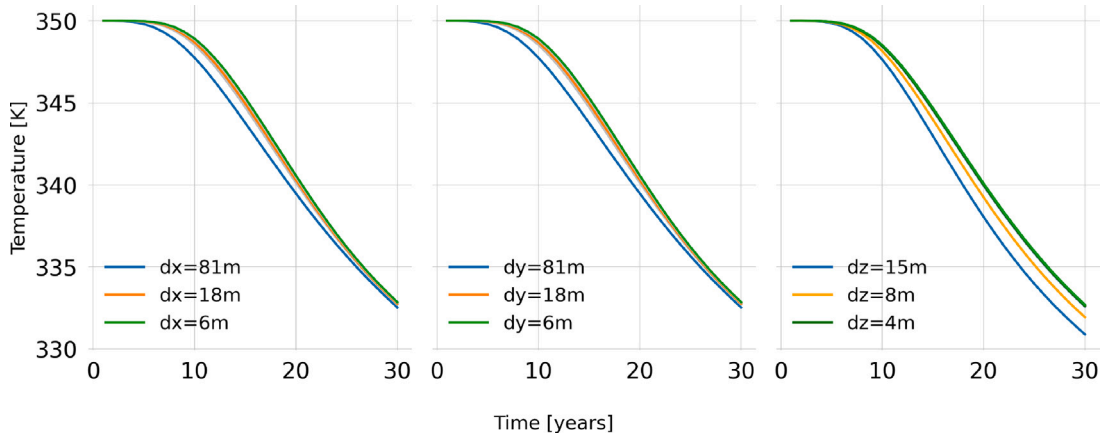

Fig. 2. Production temperature of different dx, dy and dz for a homogeneous reservoir.

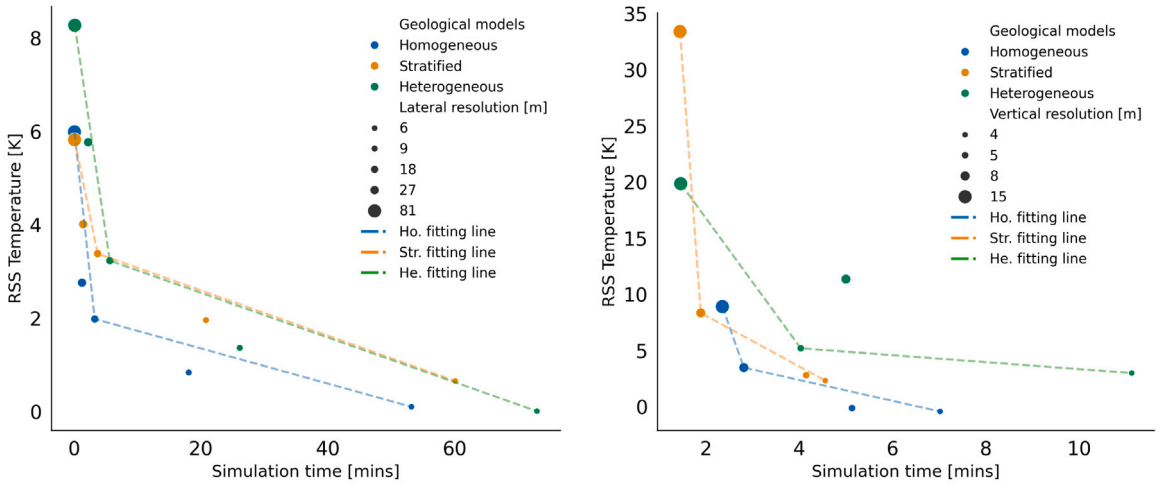

(a) Lateral resolution (b) Vertical resolution

Fig. 3. RSS of the production temperature versus simulation time subject to different dx, dy and dz for different types of reservoirs. Different colors show the geological model types, the marker size indicates dx, dy and dz values with larger markers representing lower resolution.

system. Then we employ the models with the optimal numerical setup to demonstrate a standardized approach to defining effective IA. Subsequently, we come up with a analytical method to computing the HIP recovery factor. Eventually, we show the results and discussions on the sensitivity analysis for the given geological models.

3.1. Optimal numerical setup

We first define the reference resolution as the lateral of 3 m and the vertical of 2 m. Next, we use the Residual Sum of Squares (RSS) to quantify the difference between the production temperature predicted by the reference-resolution model and that predicted by a lower-resolution model to assess the convergence of the production temperature. The temperature differences indicate the simulation's accuracy, while the elapsed simulation time serves as a measure of computational efficiency. The OCR is determined by the trade-off between the accuracy and the efficiency of given geological models. Fig. 2 gives the production temperature of a homogeneous reservoir given different resolutions in x, y, and z directions after 30 years of thermal production simulation.

3.1.1. OCR defined by production temperature

Once we obtain the production temperature of varied resolutions, we calculate the RSS of production temperature in comparison to the production temperature from the model with the reference lateral and vertical resolution. Fig. 3 shows that as the lateral and vertical resolution become closer to the reference resolution, the difference in production temperature becomes smaller, meanwhile, the simulation time increases for all three types of the geological models. After analyzing the simulation time versus RSS of production temperature, we apply the Ramer–Douglas–Peucker (RDP) (Ramer, 1972; Douglas and Peucker, 1973) algorithm with a threshold of 0.1 to efficiently find an optimal curve representation without losing accuracy. This approach, as shown in the figures (Figs. 3(a) and 3(b)), reveals that lower dz values are needed compared to dx ad dy for all models' convergence, with heterogeneous models requiring finer resolution. It means that we need a detailed vertical characterization on heterogeneity to get a converged result. While setting dx and dy to around 18 m and dz to 8–5 m, which is the intersection of two fitted lines in the graph, ensures results close to the reference solution and maintains efficiency, increasing resolution further makes simulations more cumbersome despite better accuracy.

3.1.2. OCR defined by cold plume extent volume

Considering the production temperature is a single measurement point during geothermal production, we introduce the convergence of the cold plume extent volume of the given types of reservoir to investigate the OCR. We define the cold plume extent volume as the grid block volume which has one-degree temperature drop after 30 years' simulation compared to the initial reservoir temperature. We then calculate

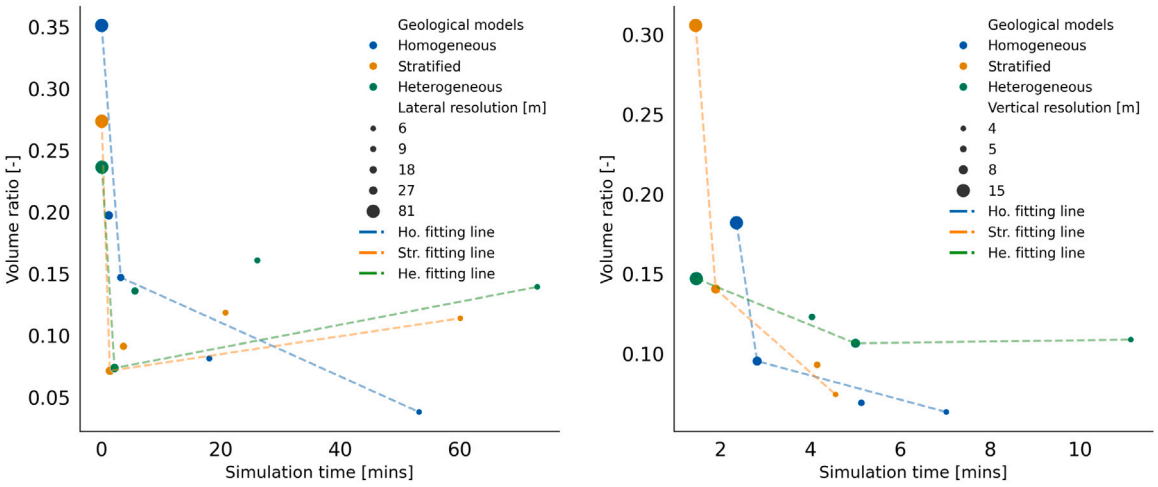

(a) Lateral resolution (b) Vertical resolution

Fig. 4. Cold plume extent volume ratio compared to the overall domain volume, subject to different dx, dy and dz for different types of geological models.

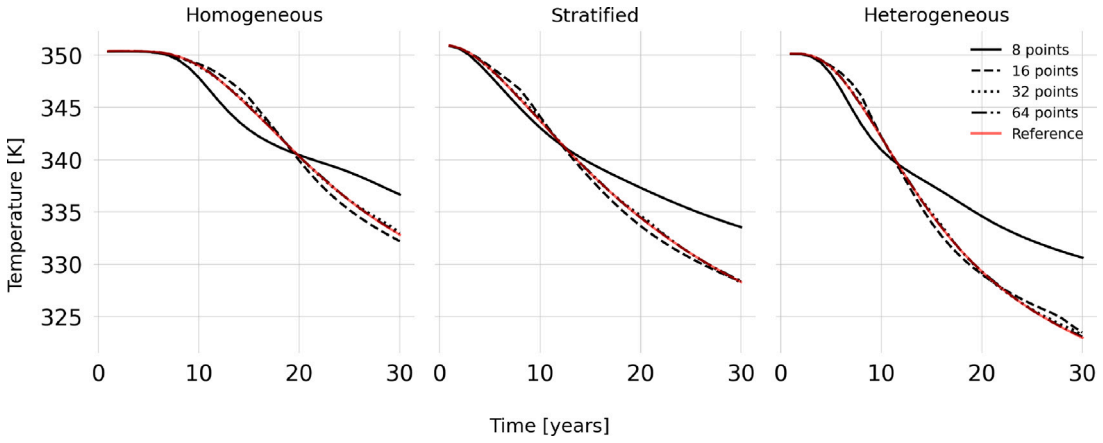

Fig. 5. The production temperature of different OBL physical resolution for the three geological models.

the volume ratio between the cold plume extent volumes of different resolutions and the total volume of the model domain. Subsequently, the difference between this volume ratio and the volume ratio from the reference lateral and vertical solution is calculated Fig. 4. Similar to Fig. 3, we incorporate fitting lines between the cold plume extent volume ratio difference and simulation time using the RDP algorithm with a threshold of 0.1. The resolution given at the intersection of the fitting lines is considered to be the OCR because the simulation accuracy is preserved while the simulation remains efficient. In general, the production temperature RSS and cold plume extent volume ratio at the intersection points from the stratified and the heterogeneous models are slightly larger compared to the one from the homogeneous model because of the combinations of the geological properties, upscaling and grid resolution alteration. However, the resolution at the intersection of two fitting lines is similar to the one we get from Fig. 3 which are a lateral OCR of 18 m and a vertical OCR in the order of 8–5 m.

3.1.3. OBL physical resolution of interpolation table

Besides the spatial resolution, the impact of OBL physical resolution of the interpolation table on the production temperature is considered in this study for different kinds of geological models (Fig. 5).

With the increase of OBL resolution, the production temperature converges for all three types of geological models. The previous study (Major et al., 2023) used 16 points for the interpolation table in low-enthalpy geothermal simulations because of the known pressure and enthalpy range. However, for a general DUGS simulation without knowing the physics range, it is better to choose 32 points, as using 16 points results in a slight difference (Fig. 5) in production temperature compared to the production temperature profile from the reference OBL resolution.

With the increase of OBL points, the RSS decreases significantly (Table 2). When the number of OBL points becomes 32, the RSS of temperature is less than one degree. The number of nonlinear iterations is proportional to the simulation time. It is obvious that after 32 OBL points, the reduction in needed nonlinear iterations slows down. Linearization cost per nonlinear iterations is minimized at 32 OBL points for all three types of geological models, however, this cost has little variation with respect to different OBL resolution. In general, the linearization cost per nonlinear iterations of the homogeneous model is lower compared to the stratified model and the heterogeneous model, meaning that heterogeneity introduces computational overhead.

Based on the convergence evaluation of production temperature and the cold plume extent volume, we decide to consider $\mathrm{dx} \times \mathrm{dy} \times \mathrm{dz} = 18\ \mathrm{m} \times 18\ \mathrm{m} \times 5\ \mathrm{m}$ as the OCR that maintains the simulation accuracy and efficiency across three types of geological models, while 32 points are chosen for the resolution of OBL physical interpolation tables.

Table 2
Simulation results from different geological models.

OBL resolution	Homogeneous			Stratified			Heterogeneous		
	Temp, RSS	Nonlinear, Iters.	Linear, per NI	Temp, RSS	Nonlinear, Iters.	Linear, per NI	Temp, RSS	Nonlinear, Iters.	Linear, per NI
8	10.5	132	11.41	14.7	146	13.02	24.1	147	13.11
16	3.0	131	11.15	2.7	135	12.66	2.9	137	12.65
32	0.7	120	11.11	0.6	122	12.40	0.8	123	12.74
64	0.2	115	11.39	0.2	117	12.42	0.2	118	12.97
128	0.05	112	11.54	0.04	115	12.74	0.04	115	13.37
Ref.	–	110	12.10	–	112	13.49	–	112	14.16

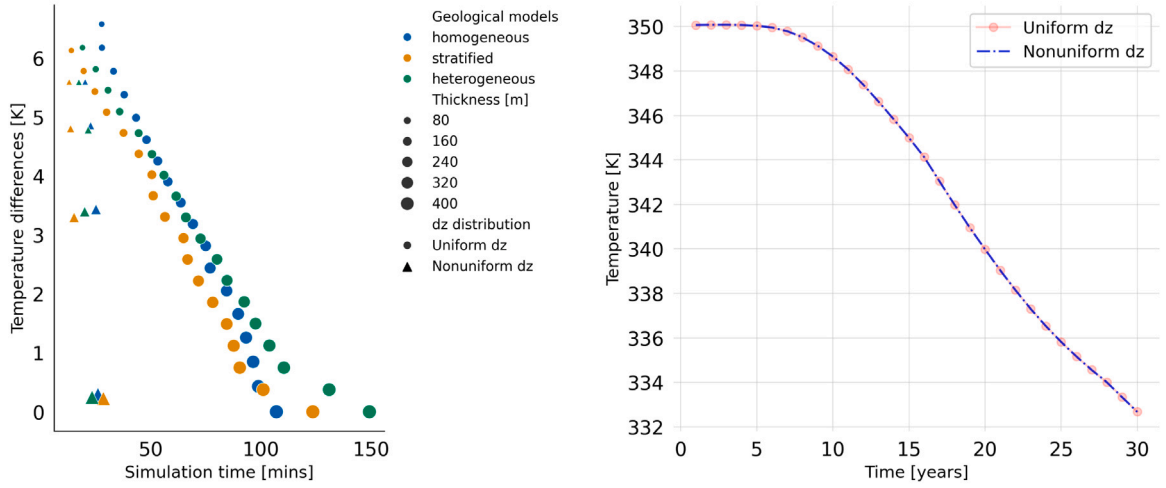

(a) Temperature difference and simulation time

(b) Production temperature

Fig. 6. The efficiency and accuracy of simulation with variation in confining layers' dz: (a) The simulation time of the case with uniform and non-uniform dz at the confining layers; (b) Production temperature of a homogeneous model with uniform and non-uniform dz at the confining layers.

3.1.4. Confining layers

We employ the models with the OCR to investigate the minimum number of confining layers (MCL) required to avoid the cold front interacting with the domain boundary. The MCL is decided if the variation of the maximal temperature and minimal temperature of the top confining layer is less than 0.05 K. We find that if the number of confining layers is larger than 76, which is equivalent to 380 m thickness on the top and the bottom of the reservoir layers, the temperature variation remains within 0.05 K.

Model resolution significantly affects the accuracy and efficiency of simulations, as discussed in Section 3.1. Fine resolution in confining layers increases computational cost despite their limited role in fluid convection. To speed up simulations while maintaining accuracy, we tested non-uniform vertical resolution (dz) in these layers. By comparing production temperature after 30 years of thermal production to a reference case which having 380 m of uniform dz confining layers, we found that non-uniform dz models achieved comparable accuracy (Fig. 6(b)) with a 3 to 4 times reduction in computation time (Fig. 6(a)). Fig. 7 shows the cold plume distribution after 30 years at the xz plane for the cases that the confining layers have uniform (Fig. 7(a)) and non-uniform (Fig. 7(b)) dz respectively.

Based on the geological models with the optimal numerical setup, we carry out the forward simulations by applying the parameters in Table 1. The 2D temperature and pressure distribution of the middle reservoir layer for three different types of the reservoirs after a 30 years simulation is shown in Fig. 8. In a homogeneous reservoir, the 2D cold plume has a slightly narrower and more regular shape compared to those in stratified and heterogeneous reservoirs. This is because permeability variations in the latter two models redirect fluid flows. Additionally, heat conduction has a greater impact in the stratified and heterogeneous models, making the cold plume extent shape more irregular than in the homogeneous model.

3.2. Recoverable HIP

TNO-AGE (2014) propose a standardized way to define effective IA of a geothermal project. However, Daniilidis et al. (2021) concluded that this definition has limitations to capture the production temperature drop. We propose a standardized approach to computing the recoverable HIP within the reservoir layers. A streamline-defined Hydraulic-Connected Area (HCA) and a Thermal-Affected Area (TAA) are used to determine the influence area of the wells. Streamlines outline the trajectory of fluid flowing from the injection well to the production well, where the tangential direction of the points on streamlines is the same to the velocity vector (Datta-Gupta and King, 2007). The HCA is the area where fluid can sweep, determined by the Time of Flight (TOF) threshold, which indicates when the fluid is capable of sweeping and draining. We define the TAA as the region where there is a one-degree drop in temperature compared to the initial reservoir temperature is observed after a certain number of years' production. It is worth noting that the size of effective IA varies for the given TOF. The grid cells within HCA and TAA determined by the same TOF are used to compute the effective IA and define the subsurface volume for computing the recoverable HIP. To demonstrate how the effective IA is defined, we set TOF to 30 years. Fig. 9 shows the effective IA of the three types of geological models based on the optimal numerical setup. Heterogeneity has a significant impact on the thermal and hydraulic behavior of DUGS. The HCA of the homogeneous and the stratified model is more uniform and similar to each other compared to the one of heterogeneous model (Fig. 9). In the stratified model, the size of the HCA varies due to the layer-wise heterogeneity of permeability, but the shape of HCA in each 2D layer is uniform. The effect of heterogeneity on the shape of HCA area becomes evident in the heterogeneous model because of the permeability variation, as shown by the irregularity of the cold plume extent. Meanwhile, the TAA of

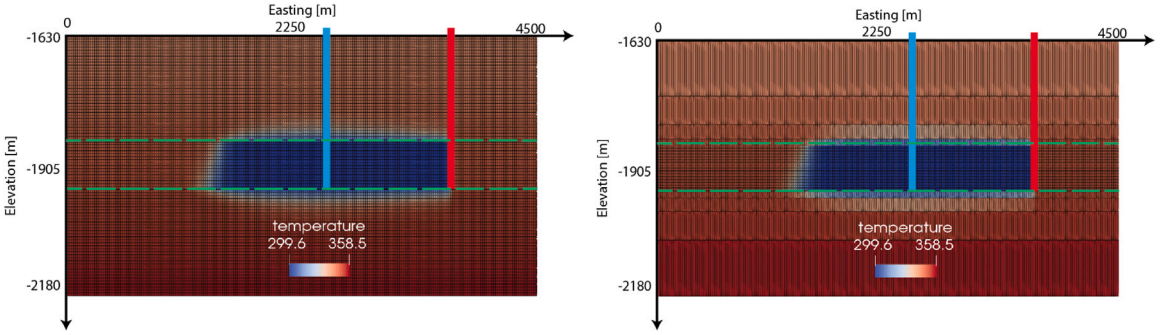

(a) Uniform dz at confining layers (b) Non-uniform dz at confining layers

Fig. 7. Temperature distribution of a homogeneous model with overburden and underburden layers at the well plane; the blue and red cylinder indicates the location of the injection well and production well respectively. The dashed green line shows the boundary between the confining layers and reservoir layers. An obvious heat flow by conduction happens between reservoir layers and confining layers.

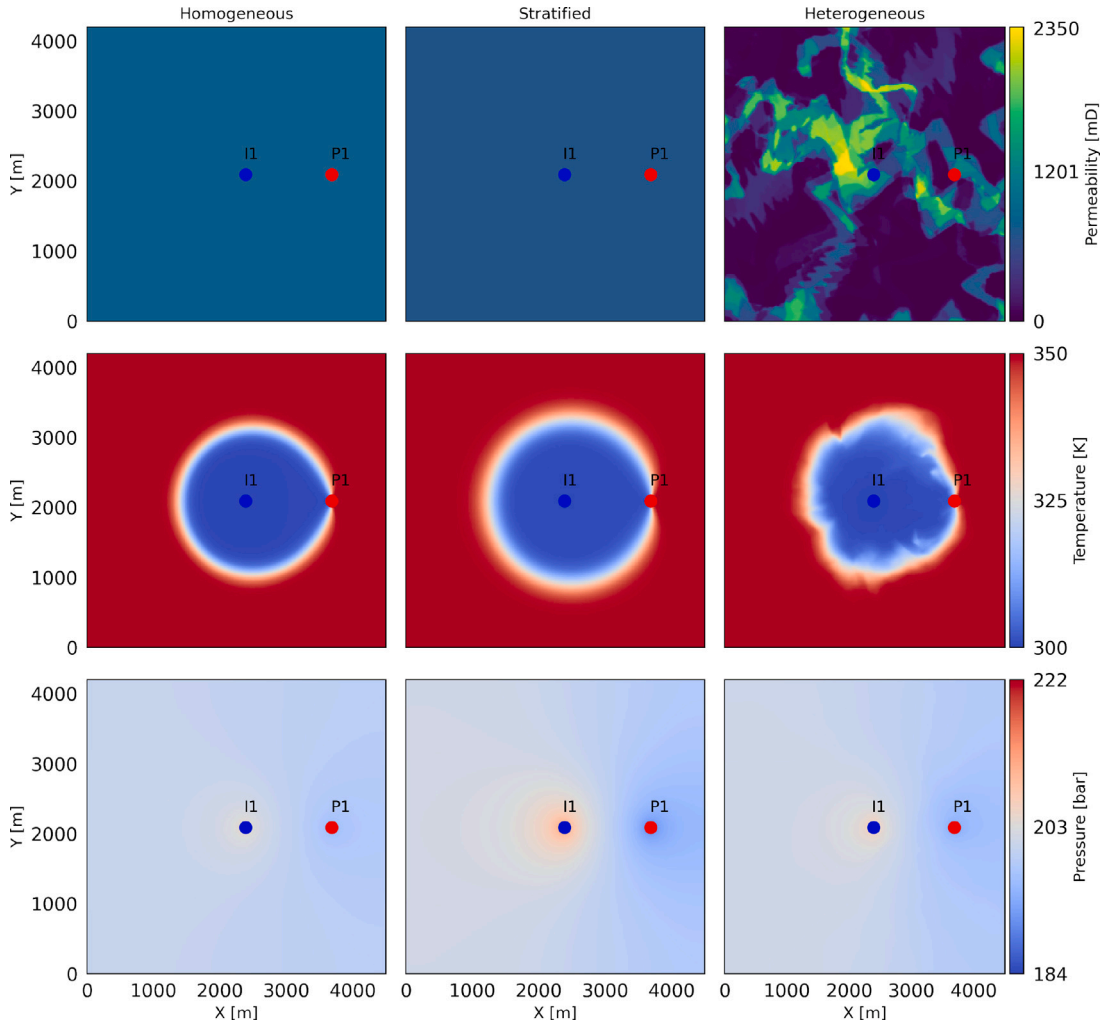

Fig. 8. Permeability, temperature and pressure distribution of the middle reservoir layer for homogeneous, stratified and heterogeneous reservoirs with the optimal numerical setup after 30 years simulation.

the stratified model and the heterogeneous model is larger than the homogeneous model's TAA. The reason is that there are both thermal conduction and thermal convection heat transfer mechanisms within reservoir layers, while thermal convection through fluid flow is the dominant heat transfer mechanism in the homogeneous model. Table 3 summarizes the recoverable HIP for the given geological models with the same total volume of 18.9×10^8 m^3.

It is important to take both HCA and TAA into account to quantify the effective IA otherwise the effective IA can be underestimated for three types of the models. The HCA of the homogeneous model is larger than that of the stratified and the heterogeneous model because the permeability of the homogeneous model is larger than the average permeability of both stratified and heterogeneous model. However, the TAA is consistently larger than the HCA for all three geological models

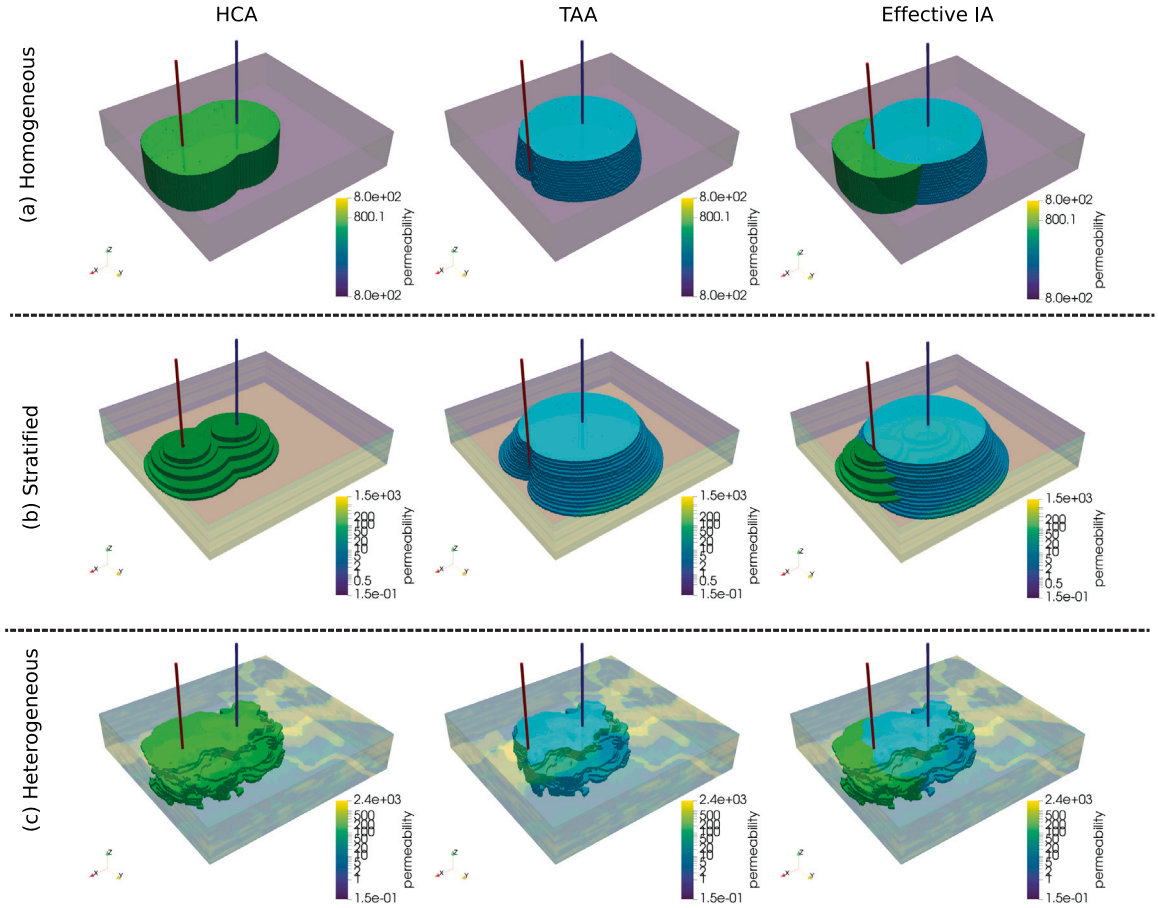

Fig. 9. Hydraulic-Connected Area (HCA), Thermal-Affected Area (TAA) and effective IA (In columns) of different geological models (In rows). The blue and red tubes are injection and production wells respectively.

Table 3
Recoverable HIP of three types of the geological models when TOF is 30 years.

	HCA [10^8 m^3]	TAA [10^8 m^3]	Effective IA [10^8 m^3]	Recoverable HIP [PJ]
Homogeneous	4.78	4.87	6.10	88.27
Stratified	3.80	6.79	7.62	102.16
Heterogeneous	3.39	5.55	6.17	84.60

because the temperature change due to heat conduction adds to the area calculation.

The effective IA covers 32%–40% of the total domain volume of the given reservoir models Table 3. Although the differences in effective IA of the stratified model is much larger than that of the homogeneous model, the recoverable HIP is similar. The effective IA difference stems from the porosity distribution of the models. The matrix volume and pore volume result in different fluid and rock internal energy. The same principle applies to the heterogeneous model which has a much lower recoverable HIP. Therefore, A proper geological characterization is required to compute correct amount of recoverable HIP. In the end, the recoverable HIP is determined solely based on the effective IA.

After we compute the recoverable HIP, we perform forward simulations using the parameters defined in Table 1 and we calculate the energy recovery factor for all three types of reservoir models. The HIP recovery factor over Pore Volume Injected (PVI) for each geological model shows a consistent behavior for different discharge rates. This consistency implies that once we know the geological model and well spacing, we can analyze the HIP recovery factor analytically for different discharge rates. The x axis of Fig. 10 is the PVI with respect to the pore volume within the effective IA. The design of our work on HIP recovery factor is accounting for the influence of discharge rate and time component for the given geological models. Fig. 10 shows that before thermal breakthrough, the HIP recovery exhibits a linear relationship with PVI across three models. The slope of the dotted lines shows that the heat recovery from a homogeneous model is faster compared to the ones from the stratified and heterogeneous model. After the thermal breakthrough, the relationship becomes nonlinear. This nonlinearity is controlled by the interplay between heat conduction and heat convection mechanisms.

3.3. Parametric study

In this section, we perform an extensive parametric study on the DUGS simulation for different types of the geological models. The reference base models, created with the optimal numerical setup, are used to investigate heat production with the simulation parameters in Table 1. The system lifetime is defined as the time when the production temperature decreased by 15% of the difference between initial production temperature (t = 0) and injection temperature:

$$T_{\mathrm{prod}_t} \leq 15\% \times (T_{\mathrm{prod}_{t=0}} - T_{\mathrm{inj}}) \tag{27}$$

Table 4 shows the parameters we consider in the parametric study.

3.3.1. Reservoir initial condition

The reservoir initial conditions are defined by the thermal gradient, pressure gradient and the depth of the reservoir; the reservoir can be initialized with the uniform pressure and temperature (Saeid et al., 2015). This work investigates the effect of uniform initial reservoir

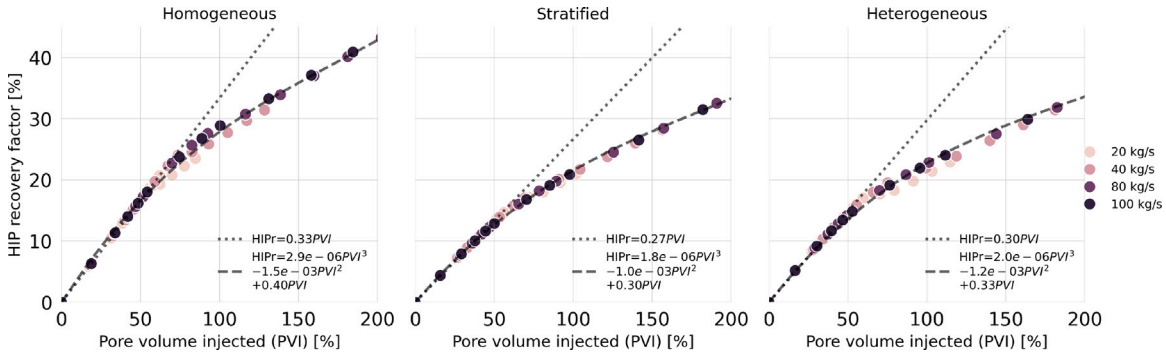

Fig. 10. Energy recovery factor of different geological models for varying PVI. Discharge rates change from 20 kg/s to 100 kg/s. Meanwhile the TOF has range between 40 years and 240 years. A nonlinear equation is applied to fit (dashed line) pore volume injected (PVI) and HIP recovery factor for each geo-model, while a linear function is used to the fit dataset before thermal breakthrough (dotted line).

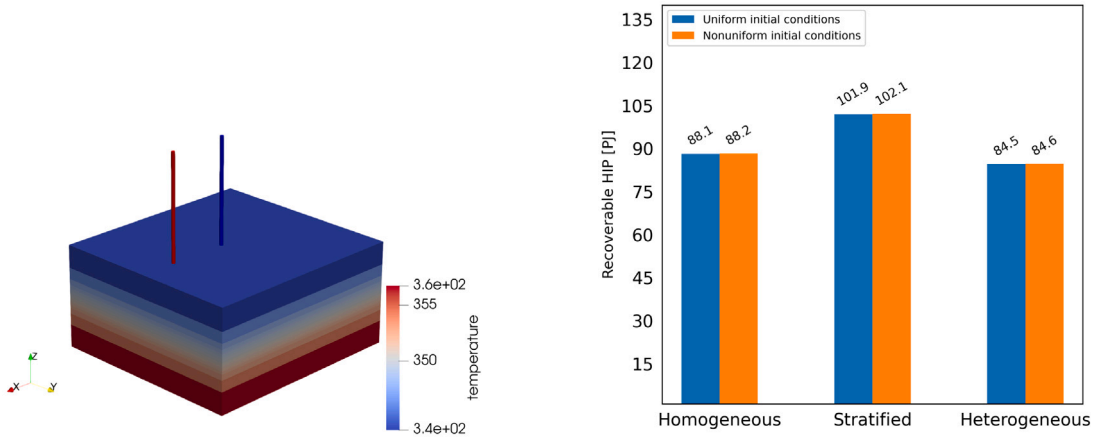

(a) Temperature (b) Recoverable HIP

Fig. 11. Different initial reservoir conditions and corresponding recoverable HIP. (a) The initial 3D temperature distribution based on the temperature gradient. (b) Recoverable HIP of different types of reservoir models with different initial conditions.

Table 4
Single parameter and values for parametric study.

Parameter name	Values
Boundary handling	[43 kg/s, 86 kg/s, Open flow geo. bnd, No flow geo. bnd]
Reservoir initial conditions	[Uniform initial condition, Non-uniform initial condition]
Salinity	[0, 3 wt%, 14 wt%, 25 wt%]
Kvkh	[0.01, 0.1, 1]
Gravity	[no gravity, with gravity]
Density	[983 $kg\,m^{-3}$, 1005 $kg\,m^{-3}$, dynamic density]
Viscosity	[0.38 cp, 0.85 cp, dynamic viscosity]
Well skin	[−3, 2, 10]

condition, namely initial reservoir pressure and initial reservoir temperature are constant, and non-uniform initial condition (base case) where both initial pressure and initial temperature are defined by the temperature and pressure gradient in Table 1 respectively. Non-uniform initial temperature distribution shows in Fig. 11(a), where the maximum and minimum temperature of the reservoir are 357 K and 344 K. Non-uniform initial conditions influence density and enthalpy of the reservoir fluid. The models with different initial reservoir conditions suggest that the variation in recoverable HIP is less than 1% (Fig. 11(b)) for the given geological models and numerical setup.

The production temperature and injection well BHP from both scenarios showing in (Fig. 12) suggests that the uniform and non-uniform initial reservoir condition has limit impact on the dynamic simulation.

3.3.2. Well skin

Different well skin factors: −3, 0 (base case), 2.0 and 10 are considered in this study. The well test from Delft Campus geothermal production and injection well indicates the well skin factor is circa 2.0 (Barnhoorn et al., 2024). It is possible to perform well stimulation to improve the effective permeability around the wellbore, which will reduce the well skin factor. This can be represented by −3 skin factor. Conversely, the instability or collapsing of the wellbore can result in a large skin value. In this work, we choose 10 as the maximum skin factor. The Fig. 13 shows the effect of skin factor.

The skin factor has little effect on the geothermal system lifetime, it has a large impact on the injection well BHP, especially at near wellbore location (Patel and Singh, 2016). The increase or decrease of a skin factor can either reduce or improve the injectivity and productivity of a geothermal well. The Peaceman well equation (Peaceman, 1983) is applied to calculate the well injectivity. Wells are controlled by constant mass rate, so skin changes are reflected in the BHP of both wells. The injection well BHP in Fig. 13 indicates that the BHP values increase significantly by more than 10% if the skin factor changes from −3 to 10 for the three types of the models.

3.3.3. Gravity effect

We keep reservoir geometry and dimension the same as other parameter's study, where the reservoir thickness is 100 m. During the simulation, the gravity option is either switched off or turned on. Fig. 14 gives the well response for the cases we enable (base case) or

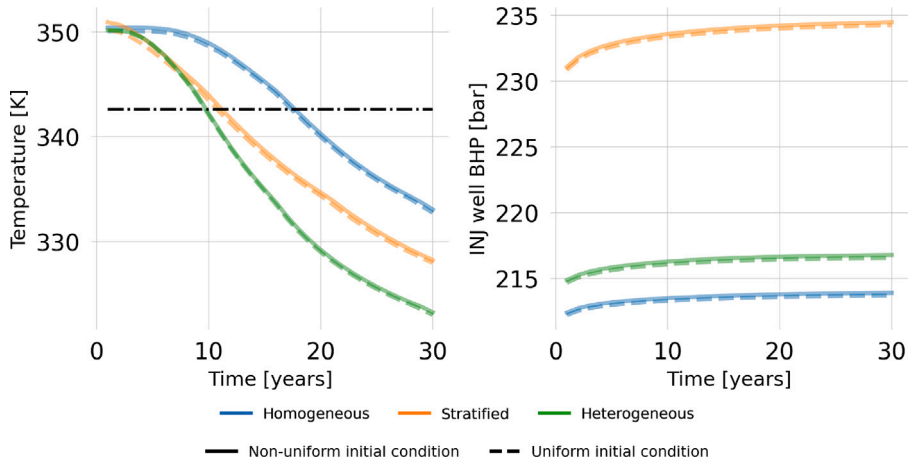

Fig. 12. Temperature and injection well BHP for different types of geological models subject to different initial reservoir conditions.

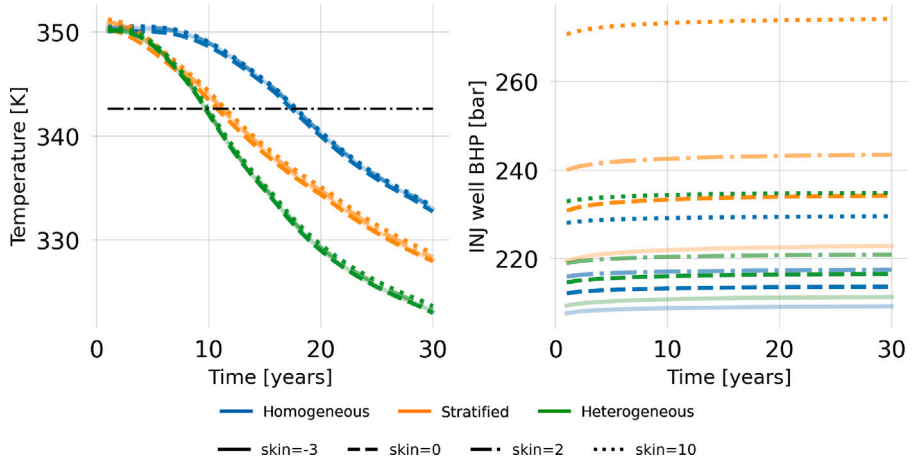

Fig. 13. Temperature and injection well BHP for different types of geological models subject to different skin factors.

disable the gravity option during the simulation. The result shows the gravity has little influence on production temperature. However, the gravity has a significant impact on the injection well BHP. Since we use mass rate control and because of buoyancy, the injection well BHP of the scenario with gravity is lower than that of the scenario without gravity. Although the reservoir thickness of all models is thin as 100 m, gravity causes the redistribution of the pressure.

3.3.4. Boundary handling

Well controls and geological boundaries are two boundary conditions in this study. All models are using the fluid mass rate well control, which are set to 43 $\mathrm{kg\,s^{-1}}$ or 86 $\mathrm{kg\,s^{-1}}$ (base case). Meanwhile, the geological boundary is established as either open flow boundary (base case) or no flow boundary. For an open flow boundary, a large volume (1×10^8 $\mathrm{m^3}$) is assigned to all grid blocks at the edge of geological models to keep the pressure and temperature at the boundary constant. Fig. 15 shows the effect of well cell boundary on the geothermal operation.

Besides well cell boundary condition, the cells at the edge of geological models can affect the performance of a DUGS. Fig. 15 shows the thermal response with respect to different geological boundary conditions. The result in Fig. 15 shows that no flow boundary gives slightly earlier thermal breakthrough for all types of the models. This implies there is no mass or energy support from the boundary cells. As the model becomes more heterogeneous, the production temperature deviates more from the base case. The injection well BHP of the stratified model with lowest permeability of 0.17 mD increases significantly during the simulation for the model with no flow boundary condition, because the pressure within reservoir accumulates during the simulation.

3.3.5. Vertical–horizontal permeability ratio

The vertical–horizontal permeability ratio (Kv/Kh) represents the hydraulic connectivity between layers. It affects the fluid flow among layers. Forced thermal convection is the main heat transfer mechanism during the development of the DUGS. However, the transverse conduction coming from temperature difference between layers also impacts the geothermal system lifetime (Tang et al., 2024). Therefore, the Kv/Kh ratio influences the thermal front propagation. For stratified model, three Kv/Kh ratios in this study are used: Kv/Kh = 0.01, 0.1, 1. This means while we keep the horizontal permeability constant, the variation is added to the vertical permeability.

An increase in the Kv/Kh ratio in heterogeneous models improves fluid communication between layers, enhancing heat sweep and lowering injection well BHP (Fig. 16). Lower Kv/Kh ratios lead to early fluid breakthrough due to limited vertical flow. In contrast, homogeneous models show minimal thermal response to changes in the Kv/Kh ratio, indicating that vertical communication has little effect on thermal production. For highly heterogeneous models, defining an appropriate Kv/Kh ratio is important to accurately represent thermal front propagation.

3.3.6. Salinity

Subsurface fluid can be categorized as fresh water (base case) to brine depending on the concentration of dissolved minerals. The range

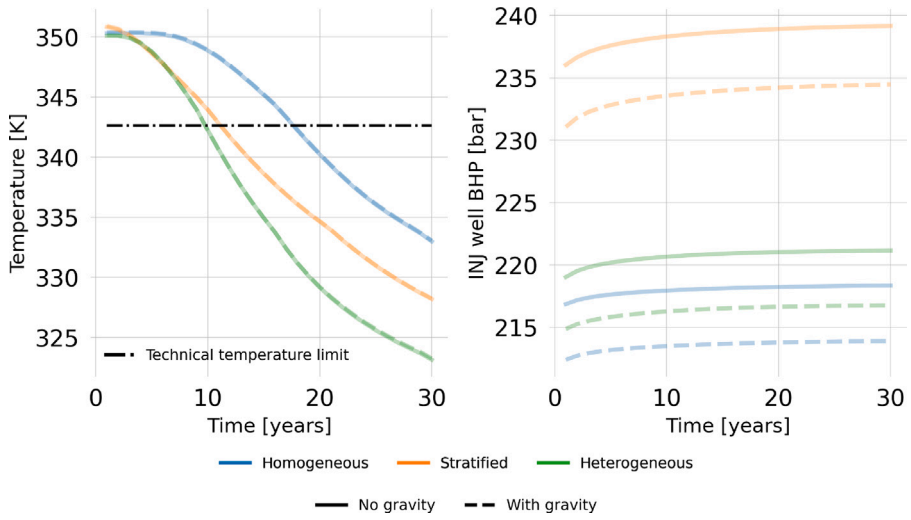

Fig. 14. Temperature and injection well BHP for different types of geological models with/without gravity.

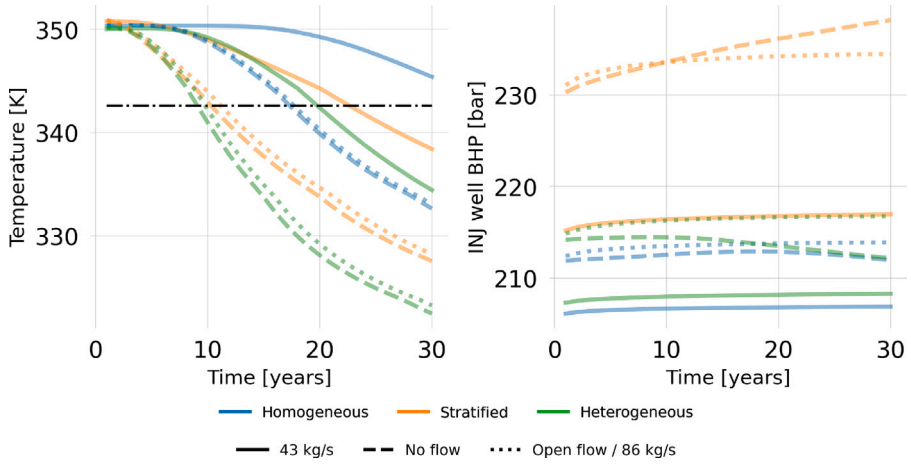

Fig. 15. Temperature and injection well BHP for different types of geological models subject to different geological boundaries: open flow boundary and no flow boundary.

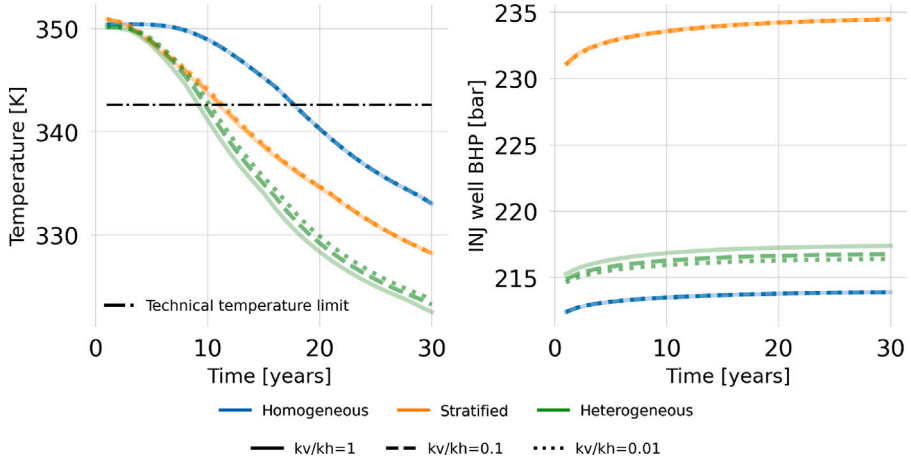

Fig. 16. Temperature and injection well BHP for different types of geological models subject to different vertical–horizontal permeability ratio.

of salinity in geothermal fluids can vary widely depending on the geological settings, the composition of formation and the depth of the formation from 0 wt% to 27 wt% (Regenspurg et al., 2010; Borgia et al., 2012; Bolourinejad and Herber, 2015; Kang and Jackson, 2016). In this study, we choose the minimum salinity of 3 wt% and maximum value of 25 wt%. The maximum value is the NaCl weight percent of the reservoir fluid near the Rotliegend reservoir, meanwhile the minimum value is the NaCl weight percent of the fluid at layers above the Rotliegend reservoir (Bolourinejad and Herber, 2015). The circulated fluid with different salinity changes the physical properties of the fluid, especially

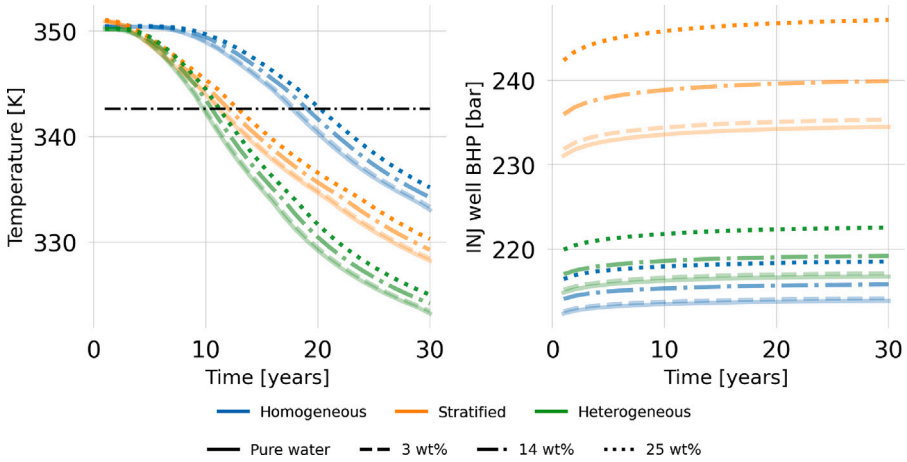

Fig. 17. Temperature and injection well BHP for different types of geological models subject to different salinity.

the viscosity (Fig. A.1). In this study, we use the correlation from Spivey et al. (2004) to compute brine density and the correlation from Mao and Duan (2009) to compute the brine viscosity as a function of salinity. The Fig. 17 shows the effect of salinity to geothermal production.

3.3.7. Temperature dependent viscosity and density

The circulated fluid's density and viscosity have an impact on the lifetime of a geothermal system. Density and viscosity of the fluid vary with temperature. We simulate the models using: (a) both density and viscosity constant, (b) constant density, (c) constant viscosity and (d) temperature-dependent density and viscosity (base case). The constant water density and constant viscosity are assumed to be 1005–983 $\mathrm{kg\,m^{-3}}$ and 0.85–0.38 cp, which are the water density and viscosity at temperature of 300 K and 350 K respectively. These changes correspond to approximately 3% in density and 55% in viscosity over this temperature range. The system lifetime becomes significantly shorter across all geological models when constant viscosity is introduced. The reason is that the main heat transfer mechanism of all models is forced heat convection and fluid flow is strongly controlled by fluid viscosity according to Eq. (1). The injection well BHP in Fig. 18 indicates at the beginning of simulation, BHP is larger compared to the base case, because the initial reservoir temperature is higher than the injection temperature (300 K), which results in a lower viscosity. As the simulation progresses, the reservoir around the injection well cools down to a temperature close to that of the injection temperature. As a result, the injection well BHP converges to a similar value across all density and viscosity variation combinations. In contrast, the constant density has little impact on the thermal response which gives a slightly shorter system lifetime and almost no change in injection well BHP.

3.3.8. Summary of individual parameters

After analyzing the impact of individual parameters, most were found to have a greater influence on the injection well BHP than on the system lifetime across all geological models. Regardless of parameter variations, the homogeneous model consistently overestimates system lifetime, based on production temperature relative to the technical temperature limit of the geothermal project, while underestimating the injection well BHP compared to the stratified and heterogeneous models. The permeability variation in heterogeneous model redistributes the fluid flow and this allows the fluid and rock to have more time to exchange heat via heat conduction to prolong the system lifetime as shown in Figs. 15, 16 and 18. Meanwhile, the geological boundary (Fig. 15) affects the production temperature profile and the effect of different boundary types on thermal response becomes stronger when the geological model becomes heterogeneous. For all models, increasing salinity (Fig. 17) has a positive impact on system lifetime, while the heterogeneity plays a limited role.

Table 5
Uncertain parameters and distributions for sensitivity analysis.

Parameter number	Parameter name	Distribution
1	Discharge rate	U[20 kg/s, 86 kg/s]
2	Reservoir depth	U[1500 m, 3000 m]
3	Geological boundary	[no flow, open flow]
4	Salinity	U[0, 30 wt%]
5	Kvkh	U[0.001, 0.1, 1]
6	Gravity	[no gravity, with gravity]
7	Density	[983 $\mathrm{kg\,m^{-3}}$, 1005 $\mathrm{kg\,m^{-3}}$, dynamic density]
8	Viscosity	[0.38 cp, 0.85 cp, dynamic viscosity]
9	Well skin	U[−3, 2.5]

The injection well BHP is largely affected by the heterogeneity. The average injection well BHP difference between a homogeneous and a heterogeneous model is more than 20 bar. Although the skin factor (Fig. 13) and gravity (Fig. 14) have insignificant influence on the production temperature across all models, they affect the injection well BHP prominently. In addition, the increase of Kv/Kh makes the flow across different layers easier, resulting in a low injection well BHP of the heterogeneous model, but a very limited impact on the homogeneous and stratified model.

3.3.9. Sensitivity analysis

Previous section demonstrates the effect of changing individual parameter while other parameters remain unchanged on the production a DUGS. This section presents the global effect of different parameters on the thermal response of DUGS using the DGSA method for the given geological models. The DGSA result is quite different compared to the result we get from varying a single parameter because of the integration and interaction of the parameters during the simulation.

The performance indicators for the sensitivity analysis are based on the system lifetime and injection BHP. We use five clusters to group the response. The uncertain inputs and their distribution are given in Table 5. Based on the parameters in Table 5, an ensemble of 1000 realizations is created for each type of geological model.

Figs. 19 and 20 show the effect of different parameters on the production temperature and injection well BHP respectively. The values of the Pareto bar are calculated based on Eq. (26). The higher the value is, the more sensitive the responses are to the input parameters. Generally, if the standardized sensitivity of a parameter is larger than 1, the parameter is considered to be important. It is worth noting that the statistical confidence interval (CI) locates at standard sensitivity equals to 1. If the Pareto bar overlaps with the CI, the parameter is considered to be critical.

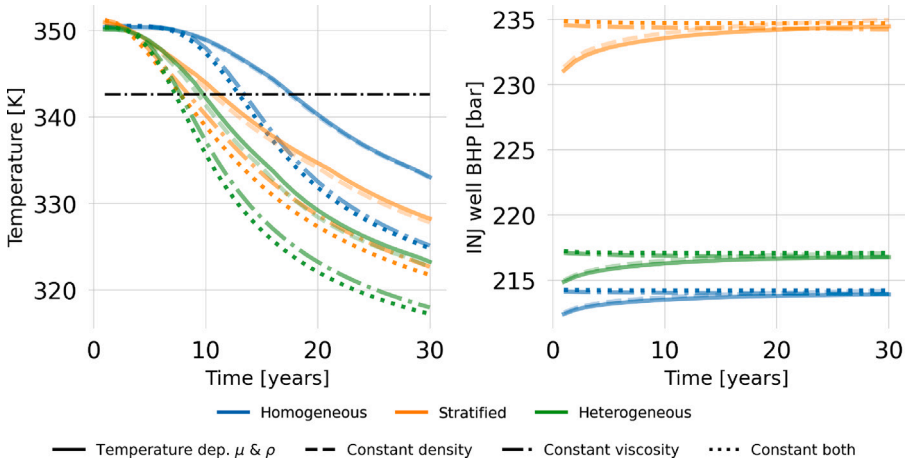

Fig. 18. Temperature and injection well BHP for different types of geological models subject to constant density, viscosity.

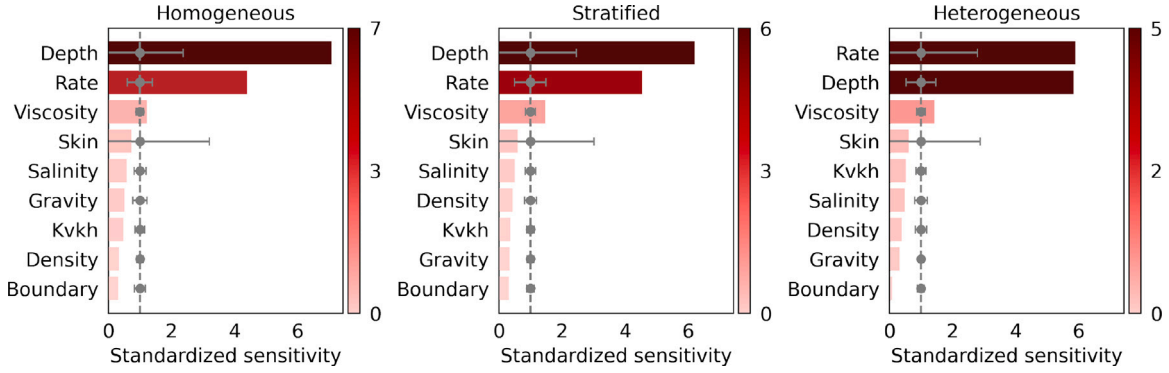

Fig. 19. Pareto plot of main effect with CI taking production temperature as a response.

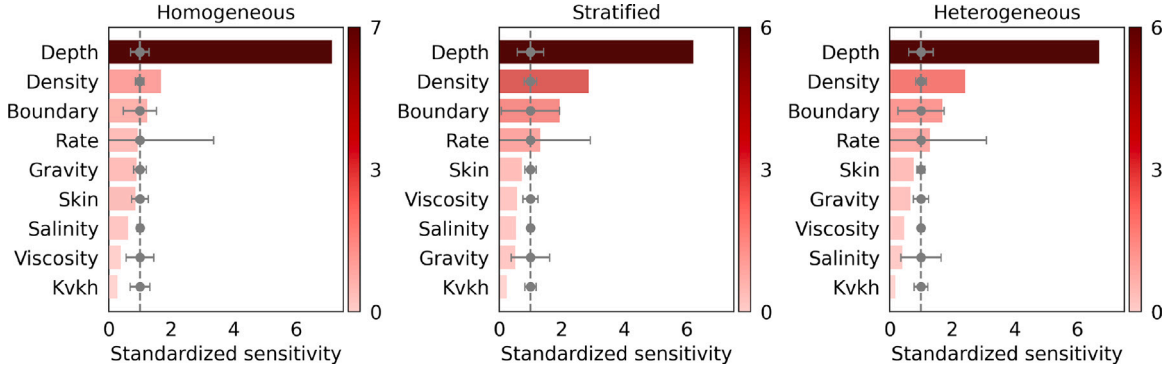

Fig. 20. Pareto plot of main effect with CI taking injection well BHP as a response.

Reservoir depth and discharge rate are considered to be the critical parameters on production temperature and injection well BHP according to this definition. The reservoir depth affects the initial reservoir temperature and initial reservoir pressure which will largely affect the production temperature and the injection well BHP because of the constant mass rate control. Meanwhile, the discharge rate also impacts the production temperature due to heat transfer being dominated by the forced convection in DUGS. The discharge rate is more sensitive when using production temperature as the response variable compared to using the injection well BHP as the response. This is because the discharge rate influences both heat convection and heat conduction throughout the entire time period, whereas the injection well BHP reaches a steady state after several years of production, which is included in the sensitivity analysis. At the same time, the geological boundary has a significant effect on injection well BHP which indicates it is imperative to consider the status of the flow from the surrounding reservoir to provide pressure support during production. However, the geological boundary has a limited effect on production temperature because the proper amount of confining layers are added to support conductive heat recharge during simulation. The viscosity of the fluid

is more sensitive while taking the production temperature as a response because the cold front movement is controlled by the viscosity. Meanwhile, density changes can affect the injection well BHP by translating the mass rate to the pressure. In contrast to previous study (Park et al., 2016), the sensitivity result shows the Kv/Kh is insensitive for all types of models while their sensitivity analysis indicates Kv/Kh ratio is an important parameter. The reason is that they dealt with a multi-phase multi-component oil-water-gas system, the fluid flow can be significantly affected by the fluid flow between layers while we are modeling a single-phase single-component water system. If we consider the dissolved gas and reactive transport in the DGSA, the result can be different.

4. Conclusions

In this study, different geological models: a homogeneous model, a stratified model and a heterogeneous model are used to define the optimal numerical setup to achieve a balance between accuracy and computational efficiency for a Direct-Use Geothermal Systems (DUGS) simulation. Subsequently, we propose a new framework to define the effective Influence Area (IA) to compute recoverable Heat In Place (HIP) for three types of the geological models. Next, we propose a framework to evaluate the HIP recovery factor of different geological models. An extensive parametric study is conducted to investigate the effect of different parameters on thermal production. We use Distance-based Generalized Sensitivity Analysis (DGSA) to assess the overall impact of the parameters in the sensitivity study. Based our results we draw following conclusions:

- The Optimal Cartesian Resolution (OCR) are defined as dx = 18 m, dy = 18 m and dz = 5 m given the limited geological data based on the convergence of production temperature and the convergence of the cold plume extent volume for three types of geological models. This OCR assures a reduced truncation error from the simulation.
- The Minimum number of Confining Layers (MCL) with an equivalent thickness of 380 m should be added at the top and the bottom of the reservoir to ensure the correct amount of heat recharge during simulation without boundary interaction. Using non-uniform cell heights for the confining layers reduces the number of burden layers from 76 to 8 without losing accuracy in production temperature.
- The Hydraulic-Connected Area (HCA) and Thermal-Affected Area (TAA) are highly affected by the average permeability of the reservoir.
- More pronounced conduction heat transfer mechanisms contribute to a larger TAA of the stratified and heterogeneous models compared to that of the homogeneous model.
- A proper geological characterization is required to accurately compute the recoverable HIP after defining the effective IA.
- The correlation of Pore Volume Injected (PVI) versus recoverable HIP are derived for three types of geological models. HIP Recovery is controlled by the geological model and is consistent as a PVI percentage for different rates.
- DGSA shows that reservoir depth and discharge rate are the two most important parameters across all geological models in DUGS development taking production temperature and injection well Bottom Hole Pressure (BHP) as the responses.
- The standardized sensitivity analysis shows that viscosity has a greater impact on production temperature than on injection well BHP. In contrast, density has a stronger influence on injection well BHP, due to the mass-to-pressure conversion, compared to its effect on production temperature.

The proposed reference geothermal DUGS simulations examples make use of the open-source software open-DARTS and are made available: https://gitlab.com/open-darts/darts-models/. They provide geoscientists, engineers and operators with different types of geological models to get preliminary ideas about the system lifetime, injection well BHP and produced energy of DUGS.

CRediT authorship contribution statement

Yuan Chen: Writing – review & editing, Writing – original draft, Visualization, Validation, Software, Methodology, Investigation, Formal analysis, Conceptualization. **Denis Voskov:** Writing – review & editing, Supervision, Methodology, Investigation, Formal analysis, Conceptualization. **Alexandros Daniilidis:** Writing – review & editing, Supervision, Resources, Project administration, Methodology, Investigation, Funding acquisition, Conceptualization.

Declaration of Generative AI and AI-assisted technologies in the writing process

During the preparation of this work the author(s) used ChatGPT in order to improve the sentences readability. After using this ChatGPT, the author(s) reviewed and edited the content as needed and take(s) full responsibility for the content of the publication.

Declaration of competing interest

The authors declare that they have no known competing financial interests or personal relationships that could have appeared to influence the work reported in this paper.

Acknowledgment

We thank Delft University of Technology for financial support and Guillaume Rongier for his insights on geological modeling.

Appendix. Fluid properties comparison between open-DARTS and other packages

Fig. A.1 shows that as salinity increases, the viscosity of the brine consistently rises at the specified temperature. In contrast, variations in salinity have minimal effect on the density of the brine.

Although we always use IAPWS-IF97 formulation for pure water geothermal production, the validation of water density and viscosity in open-DARTS shows that we obtain almost identical results compared to using IAPWS-IF97 and CoolProp. Figs. A.2 and A.3 compare the density, viscosity and enthalpy calculated from CoolProp, IAPWS-IF97 and open-DARTS for the given pressure with different temperature.

Data availability

Data and code can be found at https://gitlab.com/open-darts/darts-models/.

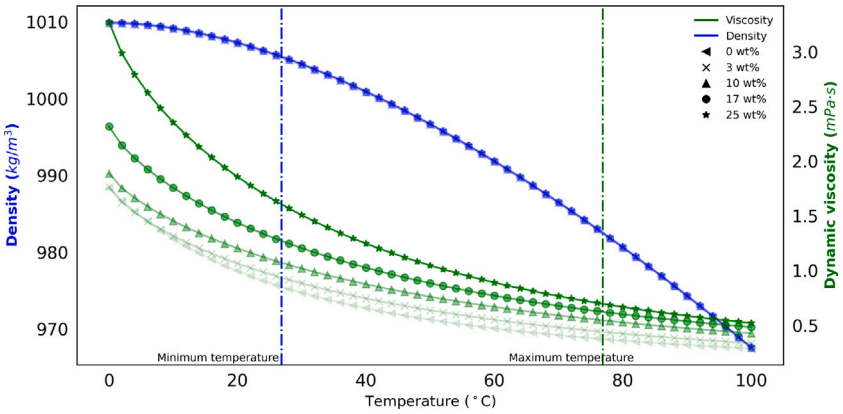

Fig. A.1. The brine density and viscosity with respect to different salinity at the pressure of 200 bar.

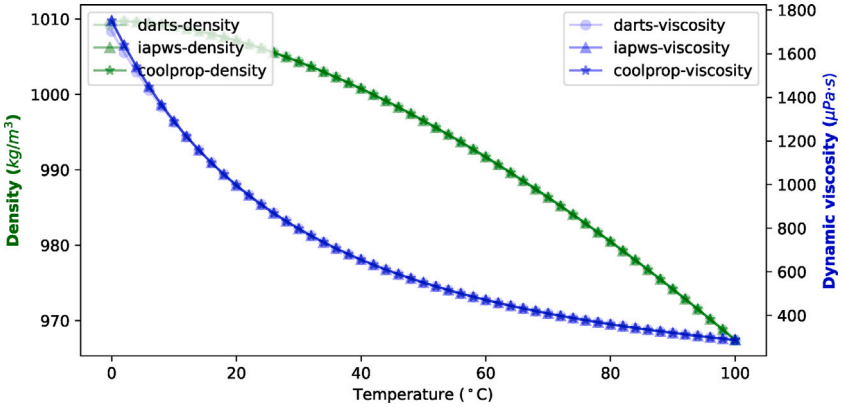

Fig. A.2. The water density and viscosity at the pressure of 200 bar.

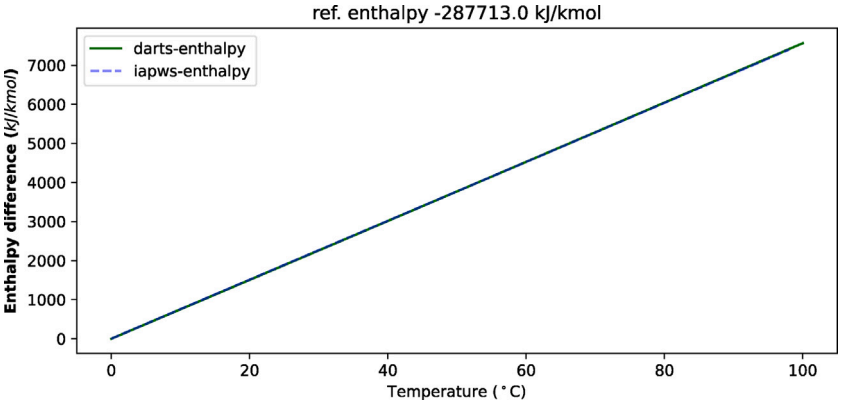

Fig. A.3. The enthalpy at the pressure of 200 bar.

References

Ahmed, T., 2010. Reservoir-fluid properties. In: Reservoir Engineering Handbook. Elsevier, pp. 29–135. http://dx.doi.org/10.1016/B978-1-85617-803-7.50010-9.

Babaei, M., Nick, H.M., 2019. Performance of low-enthalpy geothermal systems: Interplay of spatially correlated heterogeneity and well-doublet spacings. Appl. Energy 253, 113569. http://dx.doi.org/10.1016/j.apenergy.2019.113569.

Barbier, E., 2002. Geothermal energy technology and current status: an overview. Renew. Sustain. Energy Rev. 6 (1), 3–65. http://dx.doi.org/10.1016/S1364-0321(02)00002-3.

Barnhoorn, A., Vondrak, A., Laumann, S., van Esser, B., Vargas Meleza, L., Abels, H.A., Vardon, P.J., 2024. Geothermal project on TU delft campus - DEL-GT-01 and DEL-GT-02 wireline logs. http://dx.doi.org/10.4121/2A7B2A63-DD7B-46BC-A275-97729B3AB348.V1.

Battistelli, A., Calore, C., Pruess, K., 1997. The simulator TOUGH2/EWASG for modelling geothermal reservoirs with brines and non-condensible gas. Geothermics 26 (4), 437–464. http://dx.doi.org/10.1016/S0375-6505(97)00007-2.

Blank, L., Meneses Rioseco, E., Caiazzo, A., Wilbrandt, U., 2021. Modeling, simulation, and optimization of geothermal energy production from hot sedimentary aquifers. Comput. Geosci. 25 (1), 67–104. http://dx.doi.org/10.1007/s10596-020-09989-8.

Bolourinejad, P., Herber, R., 2015. Experimental investigation of porosity and permeability variations in reservoirs and caprock following co-injection of sulfur dioxide and hydrogen sulfide with carbon dioxide. J. Pet. Sci. Eng. 129, 137–144. http://dx.doi.org/10.1016/j.petrol.2015.02.036.

Borgia, A., Pruess, K., Kneafsey, T.J., Oldenburg, C.M., Pan, L., 2012. Numerical simulation of salt precipitation in the fractures of a CO2-enhanced geothermal system. Geothermics 44, 13–22. http://dx.doi.org/10.1016/j.geothermics.2012.06.002.

Bruhn, D., Taylor, N., Ince, E., Mountraki, A., Shtjefni, D., Georgakaki, A., Joanny Ordonez, G., Eulaerts, O., Grabowska, M., 2022. Clean Energy Technology

Observatory, Deep Geothermal Heat and Power in the European Union: Status Report on Technology Development, Trends, Value Chains and Markets : 2022. Publications Office.

COMSOL, I., 2023. COMSOL multiphysics. URL http://www.comsol.com/products/multiphysics/.

Crooijmans, R.A., Willems, C.J.L., Nick, H.M., Bruhn, D.F., 2016. The influence of facies heterogeneity on the doublet performance in low-enthalpy geothermal sedimentary reservoirs. Geothermics 64, 209–219. http://dx.doi.org/10.1016/j.geothermics.2016.06.004.

Daniilidis, A., 2024. Towards comprehensive uncertainty quantification in direct-use geothermal systems. In: 85th EAGE Annual Conference & Exhibition (Including the Workshop Programme). European Association of Geoscientists & Engineers, pp. 1–5. http://dx.doi.org/10.3997/2214-4609.2024101678.

Daniilidis, A., Doddema, L., Herber, R., 2016. Risk assessment of the groningen geothermal potential: From seismic to reservoir uncertainty using a discrete parameter analysis. Geothermics 64, 271–288. http://dx.doi.org/10.1016/j.geothermics.2016.06.014.

Daniilidis, A., Herber, R., 2017. Salt intrusions providing a new geothermal exploration target for higher energy recovery at shallower depths. Energy 118, 658–670. http://dx.doi.org/10.1016/j.energy.2016.10.094.

Daniilidis, A., Khait, M., Saeid, S., Bruhn, D., Voskov, D., 2020a. A high performance framework for the optimization of geothermal systems, comparing energy production and economic output. In: World Geothermal Congress 2020. Reykjavik, Iceland, pp. 1–10.

Daniilidis, A., Nick, H.M., Bruhn, D.F., 2020b. Interdependencies between physical, design and operational parameters for direct use geothermal heat in faulted hydrothermal reservoirs. Geothermics 86, http://dx.doi.org/10.1016/j.geothermics.2020.101806.

Daniilidis, A., Nick, H.M., Bruhn, D.F., 2021. Interference between geothermal doublets across a fault under subsurface uncertainty; implications for field development and regulation. Geothermics 91, http://dx.doi.org/10.1016/j.geothermics.2021.102041.

Datta-Gupta, A., King, M.J., 2007. Streamline Simulation: Theory and Practice. Society of Petroleum Engineers.

De Bruijn, E., Bloemendal, M., Ter Borgh, M., Godderij, R., Vossepoel, F., 2021. Quantifying the contribution of heat recharge from confining layers to geothermal resources. Geothermics 93, 102072. http://dx.doi.org/10.1016/j.geothermics.2021.102072.

Deutsch, C., Tran, T., 2002. FLUVSIM: a program for object-based stochastic modeling of fluvial depositional systems. Comput. Geosci. 28 (4), 525–535. http://dx.doi.org/10.1016/S0098-3004(01)00075-9.

Douglas, D.H., Peucker, T.K., 1973. Algorithms for the reduction of the number of points required to represent a digitized line or its caricature. Cartogr.: Int. J. Geogr. Inf. Geovisual. 10 (2), 112–122. http://dx.doi.org/10.3138/FM57-6770-U75U-7727.

Feng, G., Xu, T., Gherardi, F., Jiang, Z., Bellani, S., 2017. Geothermal assessment of the pisa plain, Italy: Coupled thermal and hydraulic modeling. Renew. Energy 111, 416–427. http://dx.doi.org/10.1016/j.renene.2017.04.034.

Garg, S.K., Combs, J., 2015. A reformulation of USGS volumetric "heat in place" resource estimation method. Geothermics 55, 150–158. http://dx.doi.org/10.1016/j.geothermics.2015.02.004.

Guo, B., Liu, X., Tan, X., 2017. Chapter 12 - well problem identification. In: Guo, B., Liu, X., Tan, X. (Eds.), Petroleum Production Engineering (Second Edition), second ed. Gulf Professional Publishing, pp. 329–366. http://dx.doi.org/10.1016/B978-0-12-809374-0.00012-X.

Kang, M., Jackson, R.B., 2016. Salinity of deep groundwater in california: Water quantity, quality, and protection. Proc. Natl. Acad. Sci. 113 (28), 7768–7773. http://dx.doi.org/10.1073/pnas.1600400113.

Khait, M., Voskov, D., 2017. GPU-offloaded general purpose simulator for multiphase flow in porous media. In: SPE Reservoir Simulation Conference. SPE, http://dx.doi.org/10.2118/182663-MS.

Khait, M., Voskov, D., 2018. Operator-based linearization for efficient modeling of geothermal processes. Geothermics 74, 7–18. http://dx.doi.org/10.1016/j.geothermics.2018.01.012.

Khait, M., Voskov, D., 2019. Integrated framework for modelling of thermal-compositional multiphase flow in porous media. In: SPE Reservoir Simulation Conference. SPE, http://dx.doi.org/10.2118/193932-MS.

Kong, Y., Pang, Z., Shao, H., Kolditz, O., 2017. Optimization of well-doublet placement in geothermal reservoirs using numerical simulation and economic analysis. Environ. Earth Sci. 76 (3), 118. http://dx.doi.org/10.1007/s12665-017-6404-4.

Lie, K.-A., 2019. An Introduction to Reservoir Simulation Using MATLAB/GNU Octave: User Guide for the MATLAB Reservoir Simulation Toolbox (MRST), first ed. Cambridge University Press, http://dx.doi.org/10.1017/9781108591416, URL https://www.cambridge.org/core/product/identifier/9781108591416/type/book.

Ma, R., Zheng, C., 2010. Effects of density and viscosity in modeling heat as a groundwater tracer. Groundwater 48 (3), 380–389. http://dx.doi.org/10.1111/j.1745-6584.2009.00660.x.

Major, M., Daniilidis, A., Hansen, T.M., Khait, M., Voskov, D., 2023. Influence of process-based, stochastic and deterministic methods for representing heterogeneity in fluvial geothermal systems. Geothermics 109, http://dx.doi.org/10.1016/j.geothermics.2023.102651.

Mao, S., Duan, Z., 2009. The viscosity of aqueous alkali-chloride solutions up to 623 K, 1,000 bar, and high ionic strength. Int. J. Thermophys. 30 (5), 1510–1523. http://dx.doi.org/10.1007/s10765-009-0646-7.

MATLAB, 2020. MATLAB (Version 9.9.0.1495850 (R2020b)). The MathWorks Inc., Natick, Massachusetts, United States, URL https://www.mathworks.com.

Moeck, I.S., 2014. Catalog of geothermal play types based on geologic controls. Renew. Sustain. Energy Rev. 37, 867–882. http://dx.doi.org/10.1016/j.rser.2014.05.032.

Møyner, O., Krogstad, S., Lie, K.-A., 2015. The application of flow diagnostics for reservoir management. SPE J. 20 (2), 306–323. http://dx.doi.org/10.2118/171557-PA.

O'Sullivan, M.J., Pruess, K., Lippmann, M.J., 2001. State of the art of geothermal reservoir simulation. Geothermics 30 (4), 395–429. http://dx.doi.org/10.1016/S0375-6505(01)00005-0.

Pandey, S., Vishal, V., Chaudhuri, A., 2018. Geothermal reservoir modeling in a coupled thermo-hydro-mechanical-chemical approach: A review. Earth-Sci. Rev. 185, 1157–1169. http://dx.doi.org/10.1016/j.earscirev.2018.09.004.

Park, J., Yang, G., Satija, A., Scheidt, C., Caers, J., 2016. DGSA: A matlab toolbox for distance-based generalized sensitivity analysis of geoscientific computer experiments. Comput. Geosci. 97, 15–29. http://dx.doi.org/10.1016/j.cageo.2016.08.021.

Patel, M.C., Singh, A., 2016. Near wellbore damage and types of skin depending on mechanism of damage. In: Day 1 Wed, February 24, 2016. SPE, D012S007R008. http://dx.doi.org/10.2118/179011-MS.

Peaceman, D.W., 1983. Interpretation of well-block pressures in numerical reservoir simulation with nonsquare grid blocks and anisotropic permeability. Soc. Petrol. Eng. J. 23 (3), 531–543. http://dx.doi.org/10.2118/10528-PA.

Perzan, Z., 2024. Pydgsa: a python implementation of distance-based generalized sensitivity analysis (dgsa). URL.

Poulsen, S., Balling, N., Nielsen, S., 2015. A parametric study of the thermal recharge of low enthalpy geothermal reservoirs. Geothermics 53, 464–478. http://dx.doi.org/10.1016/j.geothermics.2014.08.003.

Pruess, K., Oldenburg, C., Moridis, G., 1999. TOUGH2 USER'S GUIDE. Technical Report, Lawrence Berkeley National Laboratory.

Ramer, U., 1972. An iterative procedure for the polygonal approximation of plane curves. Comput. Graph. Image Process. 1 (3), 244–256. http://dx.doi.org/10.1016/S0146-664X(72)80017-0.

Regenspurg, S., Wiersberg, T., Brandt, W., Huenges, E., Saadat, A., Schmidt, K., Zimmermann, G., 2010. Geochemical properties of saline geothermal fluids from the in-situ geothermal laboratory Groß Schönebeck (Germany). Geochemistry 70, 3–12. http://dx.doi.org/10.1016/j.chemer.2010.05.002.

Robert, S., Pasquier, P., Nguyen, A., 2022. Impact of layered heterogeneity on thermal response test interpretation performed on a standing column well operated without bleed. Geothermics 101, 102353. http://dx.doi.org/10.1016/j.geothermics.2022.102353.

Saeid, S., Al-Khoury, R., Nick, H.M., Barends, F., 2014. Experimental–numerical study of heat flow in deep low-enthalpy geothermal conditions. Renew. Energy 62, 716–730. http://dx.doi.org/10.1016/j.renene.2013.08.037.

Saeid, S., Al-Khoury, R., Nick, H.M., Hicks, M.A., 2015. A prototype design model for deep low-enthalpy hydrothermal systems. Renew. Energy 77, 408–422. http://dx.doi.org/10.1016/j.renene.2014.12.018.

Scheidt, C., Caers, J., 2009. Representing spatial uncertainty using distances and kernels. Math. Geosci. 41 (4), 397–419. http://dx.doi.org/10.1007/s11004-008-9186-0.

Scheidt, C., Li, L., Caers, J., 2018. Quantifying Uncertainty in Subsurface Systems. American geophysical union John Wiley and Sons.

Schlumberger, 2023. ECLIPSE reservoir simulator. URL https://www.slb.com/reservoir-characterization-and-simulation/software/eclipse.

Seibert, S., Prommer, H., Siade, A., Harris, B., Trefry, M., Martin, M., 2014. Heat and mass transport during a groundwater replenishment trial in a highly heterogeneous aquifer. Water Resour. Res. 50 (12), 9463–9483. http://dx.doi.org/10.1002/2013WR015219.

Soni, B.K., 2000. Grid generation: Past, present, and future. Appl. Numer. Math. 32 (4), 361–369. http://dx.doi.org/10.1016/S0168-9274(99)00057-4.

Spivey, J., McCain, W., North, R., 2004. Estimating density, formation volume factor, compressibility, methane solubility, and viscosity for oilfield brines at temperatures from 0 to 275 ° c, pressures to 200 MPa, and salinities to 5.7 mole/kg. J. Can. Pet. Technol. 43 (7), http://dx.doi.org/10.2118/04-07-05.

Tang, J., Wang, Y., Rossen, W.R., 2024. An upscaling model for simulation of geothermal processes in stratified formations. Geothermics 122, 103095. http://dx.doi.org/10.1016/j.geothermics.2024.103095.

Thiele, M.R., 2005. Streamline simulation. In: 8th International Forum on Reservoir Simulation.

TNO-AGE, 2014. Bepaling begrenzing winningsvergunning aardwarmte. URL https://www.nlog.nl/sites/default/files/14-10.050%20ez%20%28hm%29%20bepaling%20begrenzing%20wv%20aw.pdf.

Voskov, D.V., 2017. Operator-based linearization approach for modeling of multiphase multi-component flow in porous media. J. Comput. Phys. 337, 275–288. http://dx.doi.org/10.1016/j.jcp.2017.02.041.

Voskov, D., Abels, H., Barnhoorn, A., Chen, Y., Daniilidis, A., Drijkoningen, G., Geiger, S., Laumann, S., Song, G., Vardon, P.J., Meleza, L.V., Verschuur, E., Vondrak, A., 2024a. A research and production geothermal project on the TU delft campus:. URL https://pangea.stanford.edu/ERE/db/GeoConf/papers/SGW/2024/Voskov.pdf.

Voskov, D., Saifullin, I., Novikov, A., Wapperom, M., Orozco, L., Seabra, G.S., Chen, Y., Khait, M., Lyu, X., Tian, X., De Hoop, S., Palha, A., 2024b. Open delft advanced research terra simulator(open-DARTS). J. Open Sour. Softw. 9 (99), 6737. http://dx.doi.org/10.21105/joss.06737.

Voskov, D., Zhou, Y., 2015. AD-GPRS, Stanford University's Automatic Differentiation based General Purpose Research Simulator user's manual. (Technical Report), Stanford University, URL http://pangea.stanford.edu/researchgroups/supri-b/.

Wang, Y., Voskov, D., Daniilidis, A., Khait, M., Saeid, S., Bruhn, D., 2023. Uncertainty quantification in a heterogeneous fluvial sandstone reservoir using GPU-based Monte Carlo simulation. Geothermics 114, 102773. http://dx.doi.org/10.1016/j.geothermics.2023.102773.

Wang, Y., Voskov, D., Khait, M., Bruhn, D., 2020. An efficient numerical simulator for geothermal simulation: A benchmark study. Appl. Energy 264, 114693. http://dx.doi.org/10.1016/j.apenergy.2020.114693.

Wang, Y., Voskov, D., Khait, M., Saeid, S., Bruhn, D., 2021. Influential factors on the development of a low-enthalpy geothermal reservoir: A sensitivity study of a realistic field. Renew. Energy 179, 641–651. http://dx.doi.org/10.1016/j.renene.2021.07.017.

Watanabe, N., Wang, W., McDermott, C.I., Taniguchi, T., Kolditz, O., 2010. Uncertainty analysis of thermo-hydro-mechanical coupled processes in heterogeneous porous media. Comput. Mech. 45 (4), 263–280. http://dx.doi.org/10.1007/s00466-009-0445-9.

Willems, C.J.L., Nick, H.M., Donselaar, M.E., Weltje, G.J., Bruhn, D.F., 2017. On the connectivity anisotropy in fluvial hot sedimentary aquifers and its influence on geothermal doublet performance. Geothermics 65, 222–233. http://dx.doi.org/10.1016/j.geothermics.2016.10.002.

Willems, C.J., Vondrak, A., Mijnlieff, H.F., Donselaar, M.E., Van Kempen, B.M., 2020. Geology of the upper jurassic to lower cretaceous geothermal aquifers in the west netherlands basin – an overview. Neth. J. Geosci. 99, e1. http://dx.doi.org/10.1017/njg.2020.1.

Wong, Z., Horne, R., Voskov, D., 2015. A geothermal reservoir simulator in AD-GPRS. In: World Geothermal Congress. URL https://pangea.stanford.edu/ERE/db/WGC/papers/WGC/2015/22043.pdf.

Zhang, L., Dieudonné, A.-C., Daniilidis, A., Dong, L., Cao, W., Thibaut, R., Tas, L., Hermans, T., 2025. Thermo-hydro-mechanical modeling of geothermal energy systems in deep mines: uncertainty quantification and design optimization. Applied Energy 377, 124531. http://dx.doi.org/10.1016/j.apenergy.2024.124531, https://www.sciencedirect.com/science/article/pii/S0306261924019147.